TERAHERTZ TIME-DOMAIN SPECTROSCOPY AND ITS APPLICATION TOWARDS MEASUREMENTS IN BIOLOGY

A THESIS SUBMITTED TO
THE GRADUATE SCHOOL OF NATURAL AND APPLIED SCIENCES
OF
MIDDLE EAST TECHNICAL UNIVERSITY

BY

ZEYNEP ÖZER

IN PARTIAL FULFILLMENT OF THE REQUIREMENTS
FOR
THE DEGREE OF MASTER OF SCIENCE
IN
PHYSICS

JANUARY 2016

Approval of the thesis:

TERAHERTZ TIME-DOMAIN SPECTROSCOPY AND ITS APPLICATION TOWARDS MEASUREMENTS IN BIOLOGY

submitted by **ZEYNEP ÖZER** in partial fulfillment of the requirements for the degree of **Master of Science in Physics Department, Middle East Technical University** by,

Prof. Dr. Gülbin Dural Ünver
Dean, Graduate School of **Natural and Applied Sciences** _____

Prof. Dr. Mehmet T. Zeyrek
Head of Department, **Physics** _____

Assoc. Prof. Dr. Hakan Altan
Supervisor, **Physics Department, METU** _____

Examining Committee Members:

Prof. Dr. Feride Severcan
Department of Biology , METU _____

Assoc. Prof. Dr. Hakan Altan
Department of Physics, METU _____

Assoc. Prof. Dr. Serhat Çakır
Department of Physics, METU _____

Assoc. Prof. Dr. Kıvanç Kamburoğlu
Dentomaxillofacial Radiology, Ankara University _____

Assoc. Prof. Dr. Okan Esentürk
Department of Chemistry, METU _____

Date: _____

I hereby declare that all information in this document has been obtained and presented in accordance with academic rules and ethical conduct. I also declare that, as required by these rules and conduct, I have fully cited and referenced all material and results that are not original to this work.

Name, Last Name: ZEYNEP ÖZER

Signature :

ABSTRACT

TERAHERTZ TIME-DOMAIN SPECTROSCOPY AND ITS APPLICATION TOWARDS MEASUREMENTS IN BIOLOGY

Özer, Zeynep
M.S., Department of Physics
Supervisor : Assoc. Prof. Dr. Hakan Altan

January 2016, 61 pages

Terahertz Time-Domain Spectroscopy (THz-TDS) has proved to be an exceptional tool in measurements of biological and non-biological materials. The main reason why this method is preferred is that terahertz waves are typically harmless on samples due to the low excitation energy. Furthermore, one is able to extract parameters such as the absorption and refractive index easily directly from the data without using modeling. The low energy of the terahertz wave also makes it a useful tool for characterizing dynamic behavior of a system such as done with pump/probe experiments. Also, outstanding properties of terahertz waves provide opportunity to investigate some important characteristics of biological samples like water content, vibrational spectra, and torsional modes. In this work, THz-TDS system was designed and tested using the facilities available at METU driven with an ultrafast sub 20fs Ti: sapphire mode-locked laser source. By performing experiments with the home-built terahertz time-domain spectrometer the behavior of a variety of biological materials were investigated. Specifically the studies concentrated in developing an understanding the inter-

action with terahertz radiation with hard tissues such as teeth and soft tissues such as skin. Furthermore, the interaction of the radiation with the specific amino-acid L-trytophan was also investigated.

Soft-tissue investigations focused on skin samples for development of techniques toward characterization of burn victims. Observation of changes in the burn injury's water content is one of the most important factors of the treatment. Because terahertz waves are highly absorbed by water and transparent through lots of visibly opaque materials, terahertz time-domain techniques are important to follow the healing process without removing the bandage. Burned rat-skin tissue on a glass plate was compared with glass plate with distilled drop of water underneath burned rat-skin sample and from the measurements absorption coefficients of these samples showed a large difference between 0.6THz and 1THz.

Hard-tissue studies focused on dental applications. Tooth samples, which were prepared by thinly slicing primary and adult teeth, were measured in the wet and dry states. Wet samples have higher absorption and lower refractive index compared to dry samples. In addition to that, half of the tooth samples showed signs of decay, and the refractive index as well as absorptive properties of these samples showed clear differences when compared to intact ones. Between 0.1 THz and 0.5 THz, the decayed tooth samples have lower refractive index and higher power absorption than the intact ones. Results show that there are clear differences between dentine and enamel sections of each sliced tooth. In addition, decays tend to drastically change the refractive index and absorption profile which suggests that terahertz techniques can be an invaluable tool in dentistry.

Finally, sensitivity of our measurement techniques and its potential in identifying minute concentrations of biological materials was tested in studies focused on discerning the concentration of a known biological sample in a background environment. In the first step of the concentration based L-tryptophan study, the characteristic tryptophan peaks in the frequencies of 1.42 THz and 1.82 THz in the 0.1–2 THz frequency region were observed for pure samples. The explanation of these peaks is given as the torsional motion of C11 and C12 and the ring

torsions of C1–C9 in the tryptophan molecule, respectively. When mixed with varying concentrations of polyethylene in a pellet sample, clear changes were observed in both the absorption and refractive index profiles of samples with different L-tryp to polyethylene ratios. The results show that THz-time domain spectroscopy is a useful tool to monitor the change in concentration of certain amino acids like tryptophan in a background not only the frequency domain but also in the time-domain. The measurements as outlined throughout this thesis shed light on understanding the limits and detection capabilities of THz pulsed techniques when applied to biological materials.

Keywords: Terahertz, TDS , Laser, Spectroscopy

ÖZ

ZAMAN DAYALI TERAHERTZ SPEKTROSKOPİSİ VE BİYOLOJİK ÖLÇÜMLERE YÖNELİK UYGULAMALARI

Özer, Zeynep
Yüksek Lisans, Fizik Bölümü
Tez Yöneticisi : Doç. Dr. Hakan Altan

Ocak 2016 , 61 sayfa

Zamana dayalı terahertz sepektroskopisinin (THz-TDS) biyolojik ve biyolojik olmayan malzemelerin ölçümleri için ayrıcalıklı bir gereç olduğu kanıtlanmıştır. Bu methodun tercih edilmesinin ana sebebi terhertz dalgalarının düşük uyarma enerjisinden dolayı genel anlamda zararsız olmasıdır. Buna ek olarak soğrulma ve kırılma indisi gibi parametreler modelleme kullanılmadan direk olarak veriden çıkartılabilir. Pompa/Sonda deneylerinde olduğu gibi bir sistemin dinamik davranışlarının karakterize edilmesi için terahertz dalgalarının düşük enerjisi THz-TDS'i kullanışlı bir araç haline getiriyor. Ayrıca terahertz dalgalarının önde gelen özellikleri, su içeriği, titreşim spektrumları ve burulma modları gibi biyolojik örneklerin bazı önemli niteliklerinin incelenmesine olanak sağlamaktadır. Bu çalışmada THz-TDS sistemi ultrafast sub 20fs Ti: sapphire mode-locked lazer kaynağı ile ODTÜ'de mevcut olan tesislerde tasarlanmış ve kurulmuştur. Kurulumu tamamlanan zamana dayalı terahertz spektrometresi ile gerçekleştirilen deneyler aracılığıyla çeşitli biyolojik maddelerin davranışı incelenmiştir. Çalış-

malar sırasında özellikle terahertz ışımasının diş gibi sert dokular ve deri gibi yumuşak dokular ile olan etkileşimine konsantre olunmuştur. Üstelik ışımanın L-tryptophan amino asidi ile olan etkileşimi de araştırılmıştır.

Yumuşak doku çalışmaları yanık hastalarının karakterizasyonu için tekniklerin geliştirilmesi yönünde yoğunlaştırılmıştır. Yanık yarasının sıvı miktarında gerçekleşen değişimin gözlemlenmesi tedavi sürecinin en önemli faktorüdür. Terahertz dalgalarının su tarafından yüksek emilimi ve bir çok görünürde opak olan maddenin terahertz dalgalarına transparan olması sebebiyle, zamana dayalı terahertz teknikleri iyileşme sürecini mevcut bandajı çıkarmadan da gözlemlenebilmesi için önemlidir. Cam plaka üzerine yerleştirilen yanık fare derisi ve cam plaka üzerinde yerleştirilip altında su damlası bulunan yanık fare derisi karşılaştırılmıştır ve 0.6-1THz arasında ölçümlerin soğurum katsayıları büyük bir fark göstermiştir.

Sert doku çalışmaları ise dental uygulamalara odaklanmıştır. İnce dilimlenerek hazırlanan süt ve yetişkin diş örnekleri, yaş ve kuru durumlarda ölçülmüştür. Yaş örnekler kuru örneklere göre daha yüksek soğurmaya ve düşük kırılım indisine sahiptir. Buna ek olarak, diş örneklerinin yarısı çürük başlangıcı göstermektedir ve kırılma indisi de, soğurma özellikleri de sağlıklı olan örneklere göre farklılıklar göstermektedir. 0.1-0.5 THz arasında çürük diş örnekleri sağlıklı olan dişlere gore daha düşük kırılım indisine ve daha yüksek soğurmaya sahiptir. Sonuçlar mine ve dentin tabakası arasında da net farklılıklar olduğunu göstermektedir. Ayrıca çürükler kırılma indisinde ve soğurma profilinde sert değişimlere sebep olmaktadır ve bu nedenle terahertz teknikleri diş hekimliği için değerli bir gereç olabilir.

Son olarak, ölçüm tekniklerimizin hassasiyeti ve biyolojik maddelerin çok düşük oranlardaki konsantrasyonlarının tespit edilebilmesindeki potansiyeli, bilinen bir biyolojik örneğin arkaplan ortamından ayrıştırılmasına odaklanan çalışmalar ile test edilmiştir. Konsantrasyona dayalı L-tryptophan çalışmasının ilk adımında 0.1-2 THz frekans aralığında 1.42THz ve 1.82THz frekanslarında bulunan karakteristik tryptofan pikleri saf örnekler ile gözlemlenmiştir. Bu piklerin nedenleri sırasıyla tryptophan molekülünde mevcut olan C11 ve C12 burulma hareketi ve

C1–C9 halka burulmaları olarak verilmiştir. Farklı konsantrasyonlarda polyethylene ve L-tryptophan karıştırılarak pellet örnek hazırlandığında soğurmada ve kırılım indisi profilinde farklılıklar gözlemlenir. Sonuçlar göstermektedir ki zamana dayalı terahertz spektroskopisi tryptophan gibi belirli amino asitlerin konsantarsasyon değişiminin izlenmesinde yalnızca frekans uzayında değil, zaman uzayında da kullanışlı bir gereçtir. Bu tezde özetlenmiş olan ölçümler, biyolojik malzemelere uygulandğında THz pulse tekniklerinin limitlerinin ve belirleme kapasitesinin anlaşılmasına ışık tutacaktır.

Anahtar Kelimeler: Terahertz, Zamana Bağlı Spektrometre, Lazer, Spektroskopi

To Bülent Özer and Mualla Sular

ACKNOWLEDGMENTS

I would like to thank to my supervisor Assoc. Prof. Dr. Hakan Altan for his patience and support.

I would like to thank to Hakan Keskin, he has been by my side whenever I need. His collaboration was the motivation for me.

Also, I would like to thank to Kamil Çınar and H. Mert Bozacı, it was a great pleasure to work with you.

I would like to thank to Assoc. Prof. Dr. Ingrid Wilke and Vidya Ramanathan,PhD. for sharing their experiences.

I am grateful to Esra Koruç to keep me alive during the thesis writing process.

Finally, I owe my family a debt of gratitude; K. İbrahim Özer, Sevgi Özer and, Ali Özer.

TABLE OF CONTENTS

LIST OF TABLES

TABLES

LIST OF FIGURES

FIGURES

LIST OF ABBREVIATIONS

THz	Terahertz
FTIR	Fourier Transform Infrared
PCA	Photoconductive Antenna
THz-TDS	Terahertz Time Domain Spectroscopy
TRTS	Time Resolved Terahertz Spectroscopy
FFT	Fast Fourier Transform
L-Trp.	L-Tryptophan

CHAPTER 1

INTRODUCTION

Historically, until the 1800s, light was only thought of as only comprising visible wavelengths. After the discovery of invisible forms of light it became a more general phenomenon. Although wavelengths and frequencies of various forms are different, visible light, infrared light, and ultraviolet light all derived from the same physical principles which outline the physics behind light-matter interaction.

The wave nature is evident where changes in electrical and magnetic fields cause the propagation of the light, and therefore light is referred to as electromagnetic radiation. All the possible wavelengths and frequency ranges of electromagnetic radiation are listed in the electromagnetic spectrum, Fig.1.1 [3].

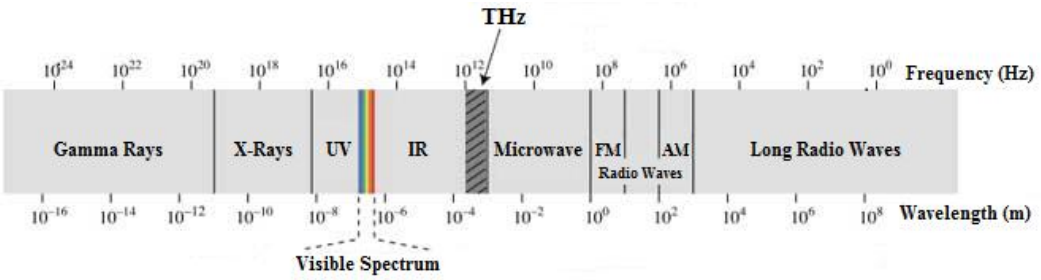

Figure 1.1: Electromagnetic spectrum

Electromagnetic spectrum does not have exact cutoff values for each region; it depends on one's reference. Gamma rays have the shortest wavelength; highest frequency, and highest energy, on the other hand, long radio waves have the

longest wavelength, lowest frequency, and lowest energy [3].

The frequency range of Terahertz waves (THz, 1 THz = 10^{12} Hz) is between microwave and far-infrared regions of the electromagnetic spectrum. All regions of the electromagnetic spectrum are used in spectroscopy. Methodology of the THz Time-Domain Spectroscopy started with the Auston switch that was invented in 1975 by David Auston [4]. Broadband THz radiation was generated by photoconductive emitter that was gated by ultra short far infrared pulses, the Auston switch, at Bell Laboratories. Spectroscopic measurements were performed with a nonlinear dielectric material and the change in time-domain was the first measurement with THz Time-Domain Spectroscopy [5, 6]. High absorption rate by water, very low photon energy, sensitivity to chemicals, transparency through lots of visually opaque materials, time-resolved feature and high signal to noise ratio of THz time-domain spectroscopy (THz TDS) are some of the main reasons that motivate the researchers about future works in THz range between 100GHz to 10THz.

1 THz corresponds to 300μm as wavelength, 33cm^{-1} as wavenumber and 4.1meV as photon energy, equal to 47.6K. With these parameters THz imaging results in sharper images as compared to microwave technology. Also, it provides better contrast for soft tissues and emits less harmful radiation levels than X-ray and ultraviolet light using applications [3, 5, 7]. Another remarkable property is the special fingerprints—absorption features, as seen in the power spectrum of the several kinds of materials in THz domain. Re-classification and characterization of the materials, that have been previously investigated and identified with other spectroscopic techniques, are some of the remarkable applications that depend on the special absorption features. On the other hand, there are some limitations in THz applications such as strong reflection by metals and strong absorption by water and other biomolecules. However, this can be turned into an advantage if the evaluation and analysis of such measurements are performed correctly.

The development of Terahertz science and technology gives rise to lots of applications. Penetration through opaque materials gives opportunities in security such as detecting threats when imaging people and inspection of sealed packages

for weapons or chemical explosives. The reflective behavior of THz from metals and special fingerprints of the chemicals in the power absorption spectrum in the THz range are the key points for developing security applications. Another emerging field is communication, where a higher frequency carrier such as THz wave can offer higher data rates than current wireless communication technologies. THz technologies are also garnering interest in biomedical diagnostics like cancer, dermatological diseases, etc. Security systems, communication systems, biomedical diagnostics (cancer, dermatological diseases, etc.), material characterization, quality control, study of historical and archaeological work are some of the outstanding fields which makes developing techniques in this range so exciting.

1.1 THz and Biology

Non-ionizing radiation with low photon energy is the most important property of THz waves for biological measurements. Effects of the ionizing radiation to water and biological molecules are harmful for biological samples. So, there is no secondary or indirect damage to biological molecules in the THz range [8, 9].

Recently, THz spectroscopy and THz imaging have started being used for the investigation of tissues and biological molecules [8]. Tissues used in THz studies could be classified into two groups: soft tissue and hard tissue. Applications of THz technology in biology are mostly used by dermatologist and odontologist for precise diagnosis [10, 11]. Recent studies have promising results with cancer tissues and dental disorders found. Proteins, medicines, and, DNA are some examples of biological molecules that are investigated in the THz range [8]. Moreover, ion concentration based measurements are performed to show the sensitivity of the THz range to biological molecules with different parameters [12].

Identification of the biological molecules with the help of the intermolecular vibrations in some of them is a remarkable method to investigate the dynamics of the large molecules [8]. Molecular rotations, low frequency bond vibrations,

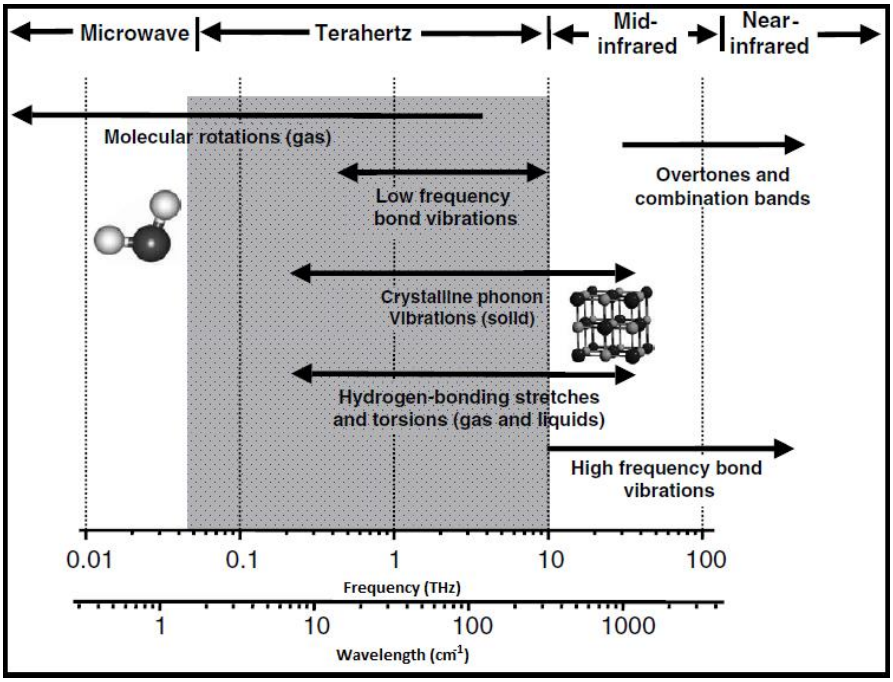

Figure 1.2: THz region for biological measurements

crystalline phonon vibrations,and hydrogen-bonding stretches and torsions are some of the characteristics of biological molecules that can be observed in the THz region [13]. In Fig.1.2 THz range of these differential features are given.

1.2 THz Generation Techniques

Naturally, with optimal environmental conditions anything could be a THz emitter as a result of the blackbody radiation. High-power level outputs are observed at higher frequencies in the power spectrum of a blackbody source,shown in Fig. 1.3. Therefore, high temperature black body emitters can be used as direct emission sources to obtain higher frequencies [14, 15].

On the other hand, weak thermal emission of the THz range is not adequate for applications like spectroscopy or imaging. Consequently, artificial sources for THz generation are used for THz technologies. Optical rectification, surface emission with semi-conductors and, photoconductive emission with antennas are the most commonly used methodologies, which depend on intense laser beams

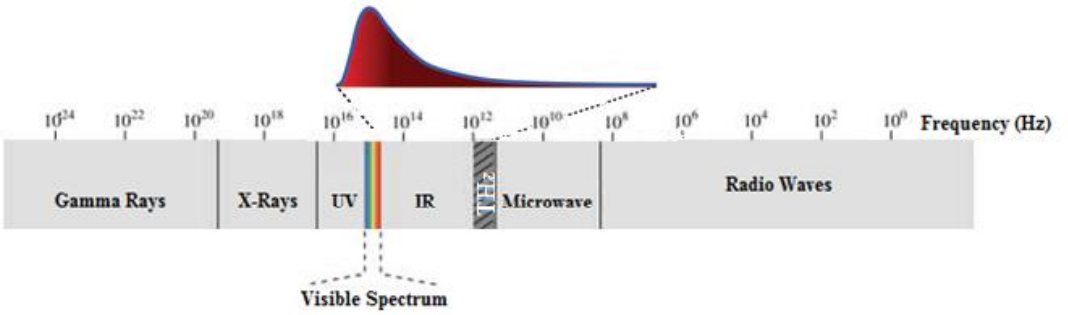

Figure 1.3: Power spectrum of blackbody sources for IR and THz regions at 100C

with ultra short pulses, to generate THz radiation [14, 15].

In optical rectification birefringent crystals, such as; ZnTe, GaP and, GaSe, are used as interaction media [15, 16]. With a birefringent structure, matching conditions for the optical group velocity and the Terahertz phase velocity become more flexible for efficient optical rectification which is the difference frequency generation, a nonlinear optical process that results in THz generation [16–18].

The theory, THz emission from the surfaces of semi-conductors depends on the bandgap width after the excitation of the surface by ultrafast laser pulses. For semiconductors with a narrow bandgap, such as; InAs and InSb, the Photo-Dember Effect explains the mechanism of THz emission with the formation of a charge dipole after the ultrafast spatial separation of electron–hole pairs in the carrier close to the semi-conductor's surface . In other respects, Surface Field Acceleration model, acceleration of photo-excited carriers in the surface-depletion field, is applicable for wide band-gap semi-conductors, for example GaAs and InP. For both cases the amplitude of the THz radiation depends on the concentration of the carriers [19–21].

Photoconductive antenna emits THz radiation with a semi-conductor chip excited by femtosecond laser pulses. Semi-conductor substrate of the chip is preferred with reference to charge carrier lifetime. Direct semi-conductor thin film with high resistivity, III-V compound semiconductors, is connected to two electrodes with a gap in between. An intense ultra-short laser pulse focused on the gap and electrodes act like a short circuit throughout the pulse duration.

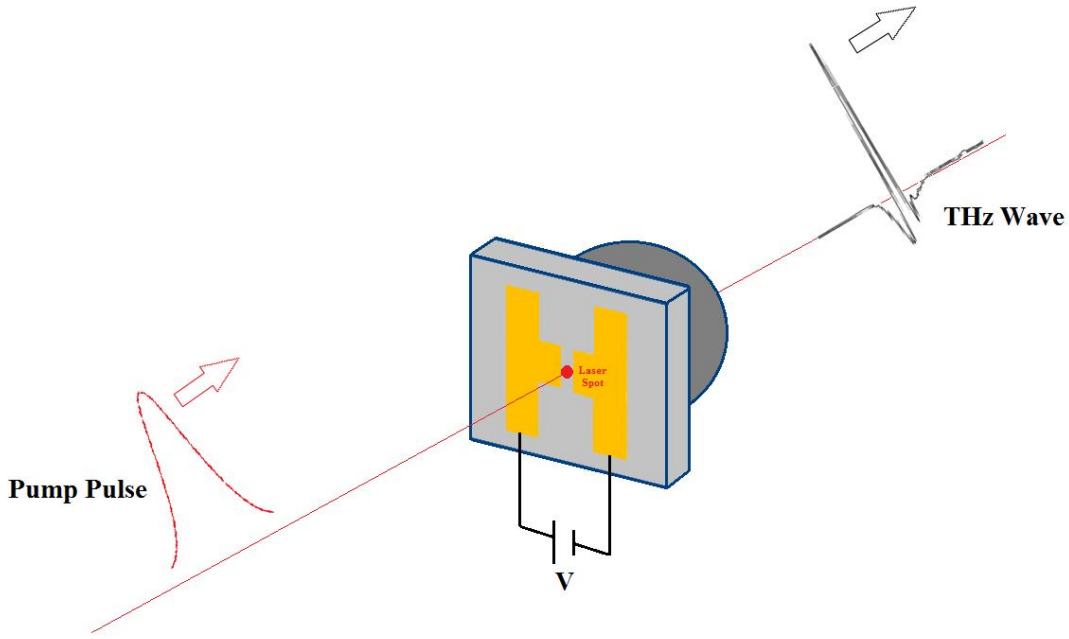

Figure 1.4: Working principle of photoconductive antenna for THz generation ; the pulse widths are not scaled.

Schematic picture of the chip with the laser spot is given in Fig.1.4. The lowest resistance of the antenna is obtained by the precise focus through the gap [22].

Photon energy of the laser pulse is larger than the gap energy of the semi-conductor. So, photons are absorbed by semi-conductor thin-film. Photon absorption by semi-conductor is resulted with a free electron in the conduction band and a hole in the valence band. After the electrodes are biased by a DC voltage, acceleration of the excited carriers is observed for a short time because of the electric field. The result of the acceleration is a rapid potential change that causes fast oscillations in the antenna afterwards. During these oscillations a wide range of THz waves are emitted and the distribution of the THz waves is provided with the help of the silicon lens [23].

1.3 THz Detection Techniques

Photoconductive detection and electro-optic sampling are the most common THz detection techniques.

The working principle of photoconductive antennas is similar for detection and generation mentioned in the previous section. During photoconductive detection the probe pulse falls onto the semi-conductor chip of the antenna and the THz wave focuses onto the silicon lens of the antenna, shown in Fig. 1.5 [24].

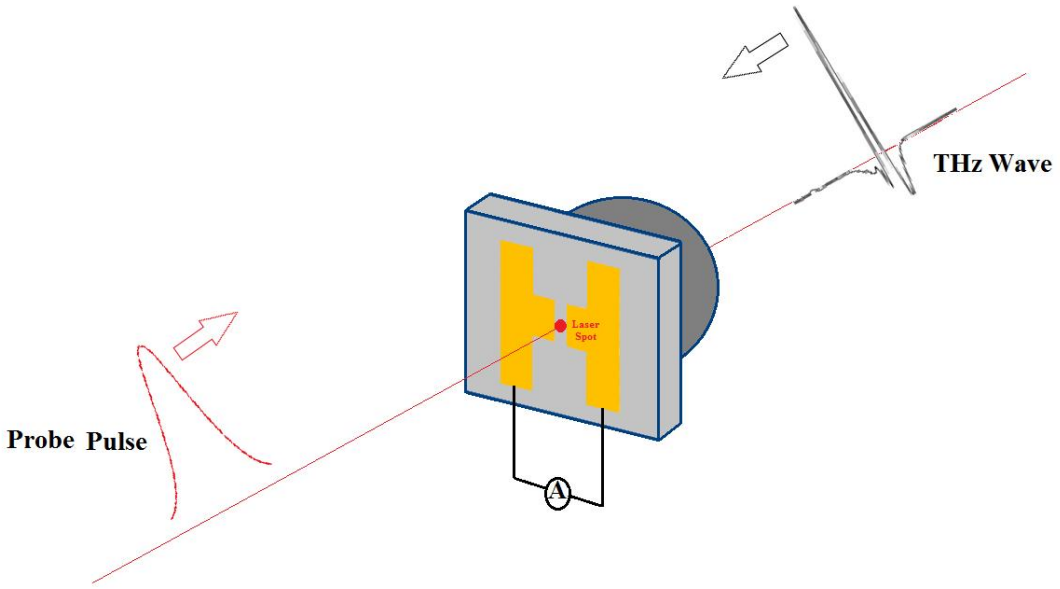

Figure 1.5: Working principle of photoconductive antenna for THz detection; the pulse widths are not scaled.

Pockels effect, describes the birefringence in an optical medium induced by an applied electric field, is the starting point of Electro-Optic Sampling. The birefringence in an electro-optic medium is modulated by the incident THz pulse and proportional to the electric field of the THz pulse in the case of THz spectroscopy [25]. In Fig. 1.6 basic working principle of the method is given. After the interaction of the optical pulse and THz pulse in ZnTe crystal, a quarter-wave plate is used for polarization control and with a Wollaston prism the beam is divided into two separate polarization states and finally horizontal and vertical components of the elliptical polarized beam is measured with a balanced

photo-detector. In section 2.1.2 Electro-Optic Sampling will be investigated in more details.

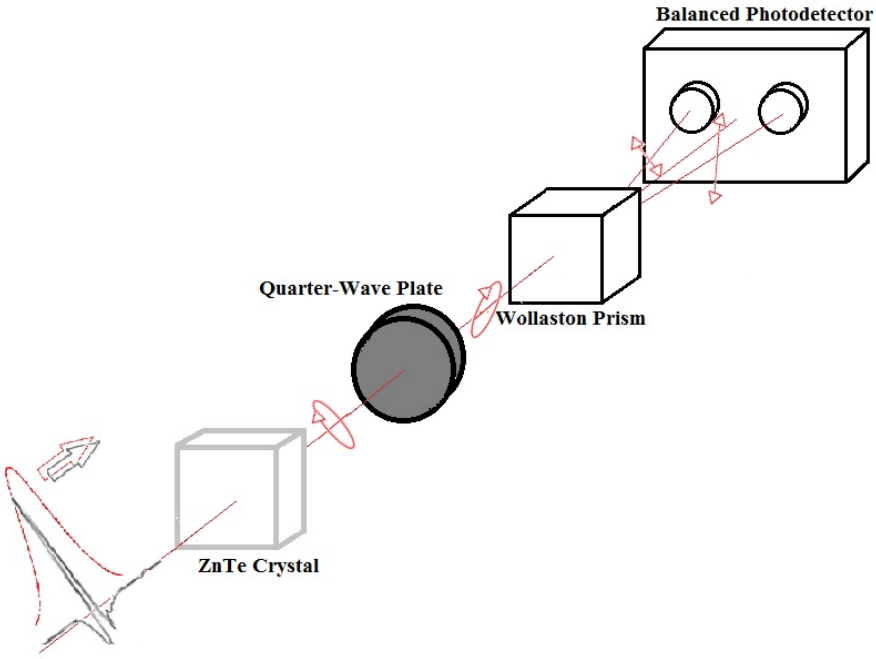

Figure 1.6: Working principle of the method of Electro-Optic Sampling; the pulse widths are not scaled.

A quarter wave plate is used for the measurement of the probe beam before the detector in both methodologies. With the measurement of the time delay between the probe pulse and the THz signal and the change in DC current of the antenna, the electric field in the time domain and the THz waveform are obtained [24].

1.4 Time-Domain and Time-Resolved THz Spectroscopy

Coherently and synchronously THz wave generation and detection by using visible or near-IR laser pulses are the fundamental principles of THz spectroscopy that contains the measurements in the frequency range of 0.1 to 100 THz [26].THz Time-Domain Spectroscopy (THz-TDS) and Time-Resolved THz Spectroscopy (TRTS) are the most common preferred methodologies for biological measurements in THz region. In THz spectroscopy systems detection and

generation of THz waves are provided by the same laser beam. With the help of a beam splitter, the laser beam is divided into two with respect to the required power.

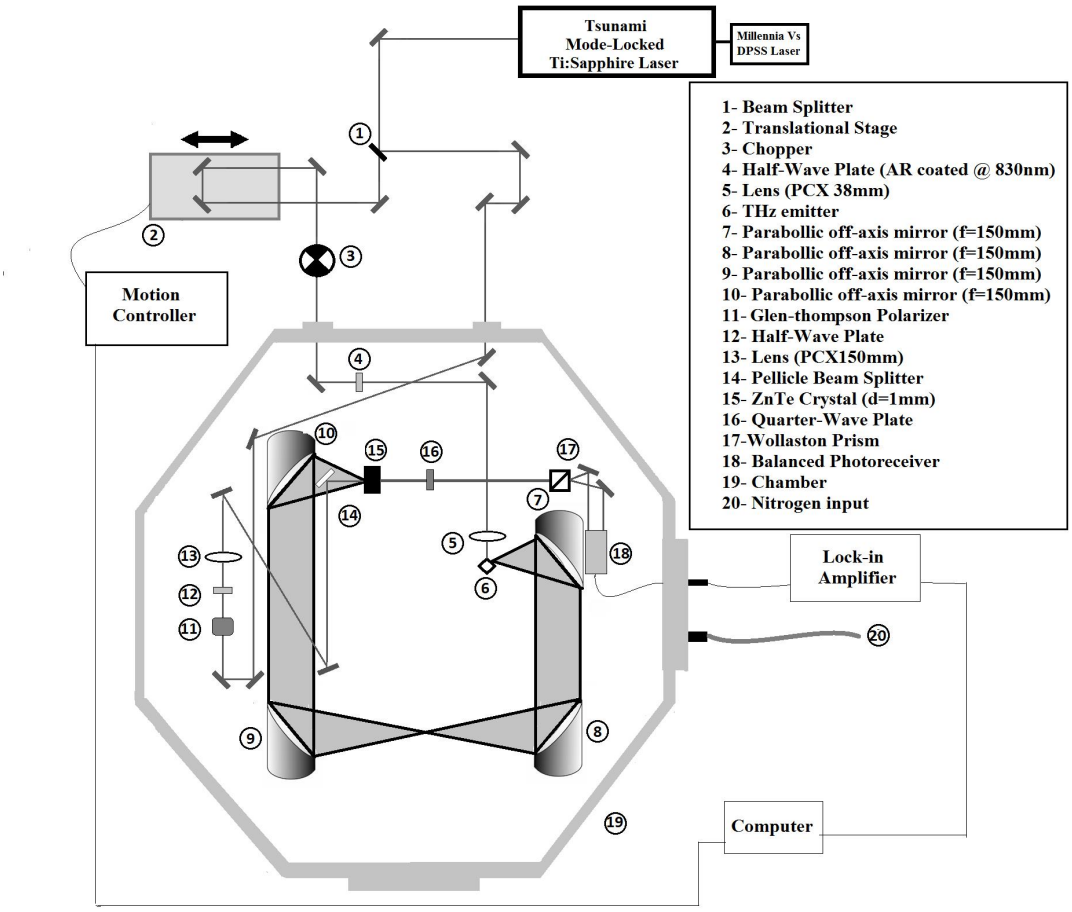

Figure 1.7: THz-TDS System in Center for THz Research, RPI

Performing the measurements with a THz-TDS system is the most effective and fastest methodology for the analysis of the complex refractive index of a material over a broadband frequency [27]. In case of THz-TDS there are only generation and detection arms, labeled as pump and probe arms, respectively.

The gradient in the electric field of the THz wave due to transmission through the sample is obtained from the detector as a time dependent data. System properties will be elaborated on Chapter 2. Afterward, the time dependent data with and without the sample is converted to the frequency dependent data

using Fast Fourier Transform. The analysis of the time and frequency dependent data with and without the sample resulted with the complex refractive index and absorption features of the material [27]. In Fig.1.7 THz-TDS system that was used in Center for THz Research, Rensselaer Polytechnic Institute is given. THz emission from the surfaces of a semi-conductor is measured by electro-optic sampling.

The effects of the photo-induced changes to the amplitude and phase of the THz wave could be measured with the temporal resolution higher than 200fs in Time-Resolved THz Spectroscopy [28,29]. In TRTS system, that was developed in UNAM, Bilkent University, ZnTe crystal is used for the generation by optical rectification and photoconductive antenna for detection, Fig. 1.8. In addition to the detection and generation arms of the system, there is a third beam path for the excitation of the sample known as the pump arm in TRTS and it is shown with the color red in Fig. 1.8 [30]. With the translational capability of these arms, different kind of scanning techniques are provided; 1D probe scan, 1D pump scan and, 2D scan. With 1D scans average dynamics in the frequency domain of THz pulse is measured. 1D pump scan is used to obtain the data about the average THz absorption by sample. However, in the case of changing refractive index or frequency dependent transient absorption 2D scan is needed to have adequate knowledge about the dynamical process. 2D scan could be applied in two different combinations of the arms' mobility conditions. The status of the detection, generation and pump arms during the 1D probe, 1D pump and, 2D scans are summarized in Table 1.1 [28,29].

The aim of this work is the detailed investigation and analysis of the biological measurements with a THz-TDS system that contains a photoconductive antenna for generation and a ZnTe crystal for detection by the method of electro-optic sampling. During the selection of the biological samples, the interactions between the THz wave and hard tissues and soft tissues were considered to investigate the material interactions of THz waves in biology. Teeth and skin samples are classified as hard tissue and soft tissue respectively. Furthermore, the sensitivity to the intermolecular vibrations is studied with different concentrations of specific amino-acid L-trytophan.

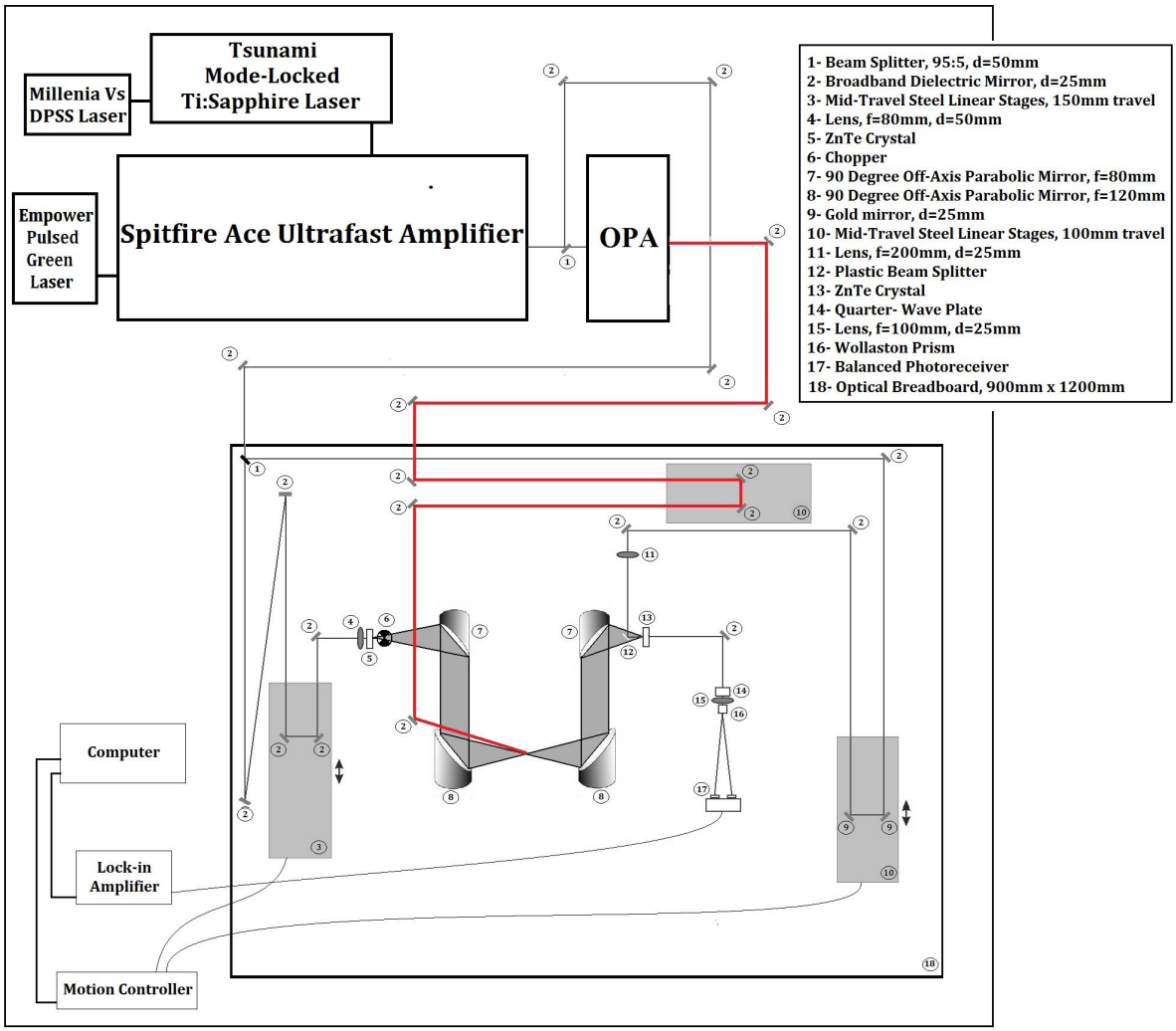

Figure 1.8: TRTS System in UNAM, Bilkent University

	1D probe scan	1D pump scan	2D scan	
			(i)	(ii)
Detection Arm	**SCAN**	**FIX**	**FIX**	**SCAN (Synchronized)**
Generation Arm	**FIX**	**FIX**	**SCAN (Reverse)**	**FIX**
Pump Arm	**FIX**	**SCAN**	**FIX**	**SCAN (Synchronized)**

Table1.1: Summary of the 1D and 2D Scans in TRTS

In Chapter 2 measurement and analysis methodologies of THz-TDS are explained in particular to the system that the experiments are performed with. In the following chapter background information about the biological samples, methods that are applied during the preparation phase of the samples and, results of the THz-TDS measurement are classified and explained into three main subtopics; hard tissue measurements, soft tissue measurements and, amino acid measurements. Finally, the summary of the work and the discussion of the future works that could be developed with the results of this thesis are given in the last chapter.

CHAPTER 2

MEASUREMENT AND ANALYSIS METHODOLOGIES OF THZ-TDS

Main principle of THz-TDS is the generation and detection of THz waves. There are various methods to generate THz waves and detect the THz signal. These methodologies are briefly explained in Chapter 1. Time dependent data is gathered with the detection of the transmitted THz waveform with and without a sample and then with the Fast Fourier Transform, frequency dependent data is obtained. With the thickness of the sample material parameters are extracted from the time and frequency domain data.

2.1 THz Time Domain Spectroscopy

Optical rectification with electro-optic crystals, surface emission with semiconductors and photoconductive generation with antennas are the main methodologies for THz generation. Electro-optic sampling or photoconductive antenna detection are the options for THz detection. In this work THz generation with photoconductive antenna and THz detection with electro-optic sampling are used.

2.1.1 THz Generation with Photoconductive Antenna

Photoconductive antenna, an optical excited broadband Terahertz emitter and detector, consists of three main parts; semi-conductor chip, silicon hemispherical

or hyper-hemispherical lens and, holder. THz generator and THz emitter parts of the antenna for generation are given in Fig.2.1 [31].

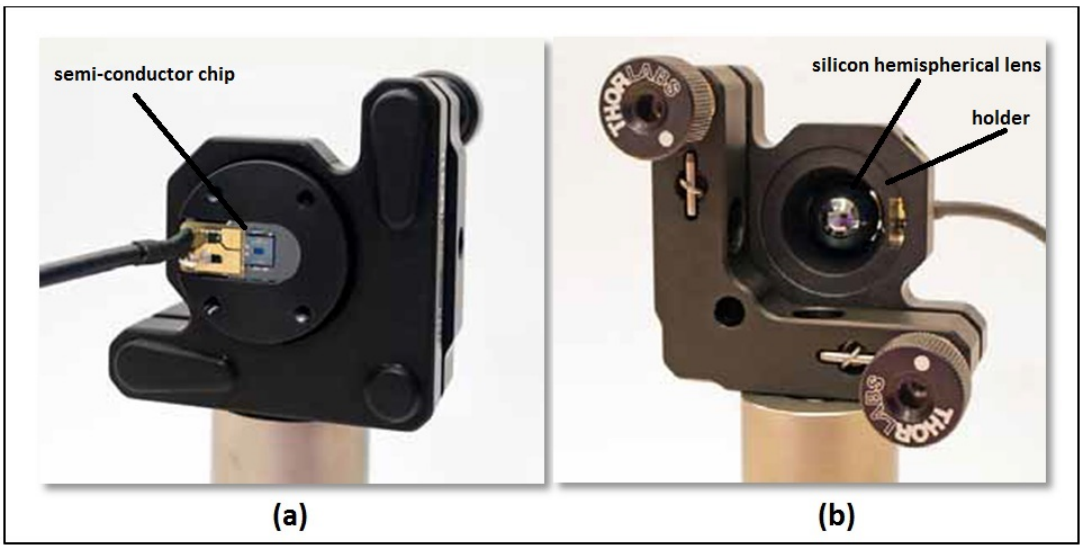

Figure 2.1: (a) THz generator and (b) THz emitter sides of the photoconductive antenna [1]

Some of the important parameters for photoconductive antennas are the gap distance (g), the length (l) and the gap width (w), as shown in Fig.2.2. The gap of the distance is important for the laser excitation, the length specifies the emitted THz resonance frequency and, the width affects on the amplitude of the detected signal [1,32].

Different geometrical structures have been used to achieve higher output powers for photoconductive antennas. Butterfly antenna, parallel line antenna, bow-tie antenna, iPCA - large area interdigital array, bow-tie antenna with finger gap and, SPCA - logarithmic spiral antenna are some of the examples [32]. In this study only iPCA - large area interdigital array antenna was used as the THz emitter [31].

2.1.1.1 Large Area Interdigital Photoconductive THz Antenna

The structure of the large area interdigital antennas is developed by using more advanced technology than above mentioned photoconductive antenna. An extended gap, with only 5 μm gap distances, along the gold finger electrodes has

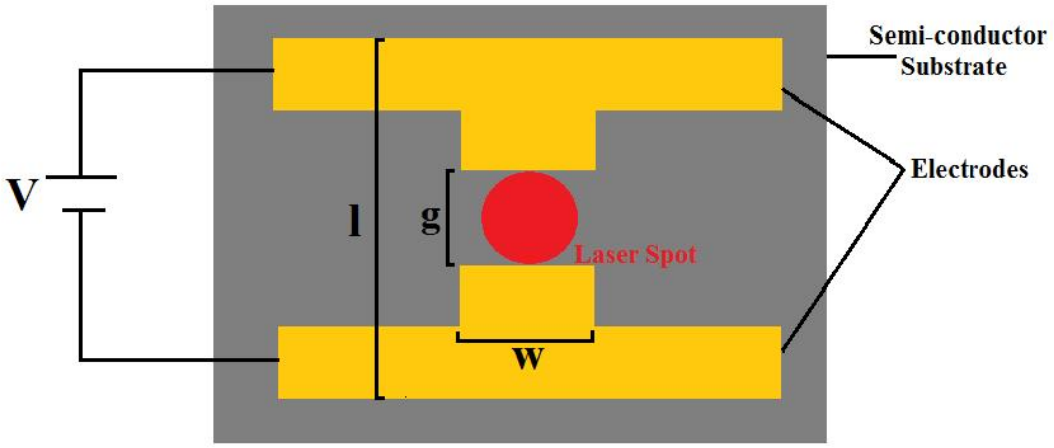

Figure 2.2: Position of the laser spot on the chip schematically

great advantages compared to only one gap. Also, in front of the chip there is a fused silica microlens array to focus on the gaps. With help of the microlens array the illuminations of the gaps are maximized and the energy usage for the excitations is almost equal to the total optical laser energy excitations of the carriers. Furthermore with the prealigned hyper-hemispherical silicon lens THz waves are dispersed with a large solid angle [31].

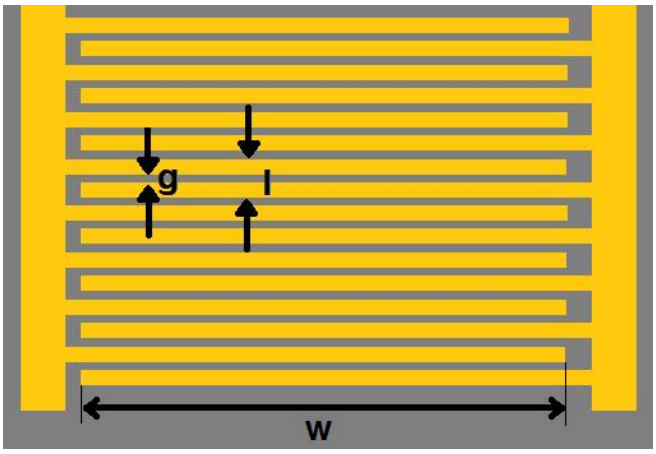

Figure 2.3: Schematic representation of the gap distance (g), the length (l) and the gap width (w) of the large area interdigital photoconductive THz antenna

GaAs chip of the antenna is given in Fig. 2.4. Active area of this chip is 1mmx1mm and its emitted THz spectrum is between 0.1-4THz. When the

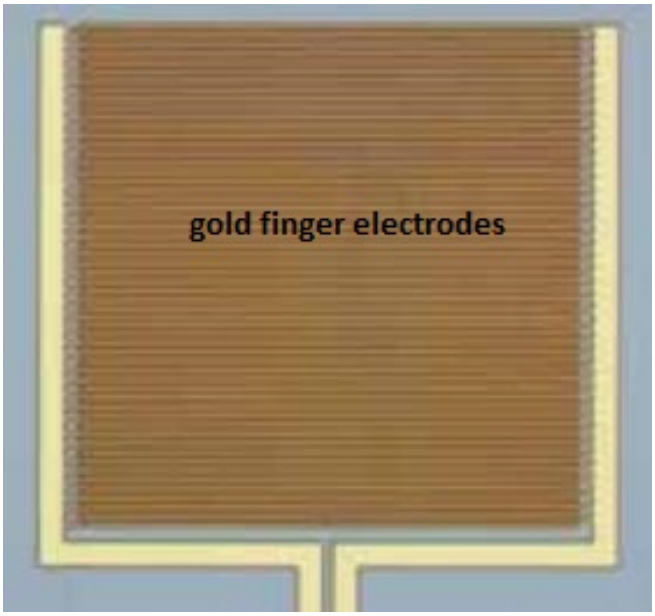

Figure 2.4: GaAs chip of the large area interdigital photoconductive THz antenna [1]

ultra-short pulsed laser beam is focused on the chip, with the microlens array only one of the two gaps is illuminated through the finger electrodes. Working principle of the microlens array is shown in Fig.2.5. Each illuminated gap excites coherently and acts like individual THz emitters that result in a constructive interference [31].

The definitions of the parameters, like the gap distance (g), the length (l) and the gap width (w), are same with only one gap conditions and they are valid for each gap through the gold finger electrodes. These parameters are shown on a schematic representation of the finger electrodes in Fig. 2.3

The results of the reference measurement that was performed with iPCA - large area interdigital array antenna in THz Research Laboratory, Department of Physics, METU, are given in 2.6. Power spectrum range was observed between 0.1THz-2THz.

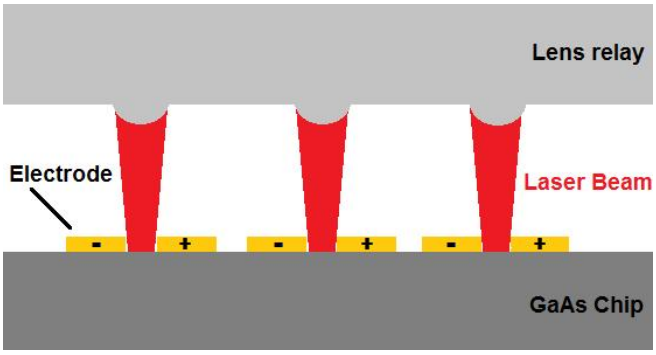

Figure 2.5: Transmission of the laser beam through the microlens array

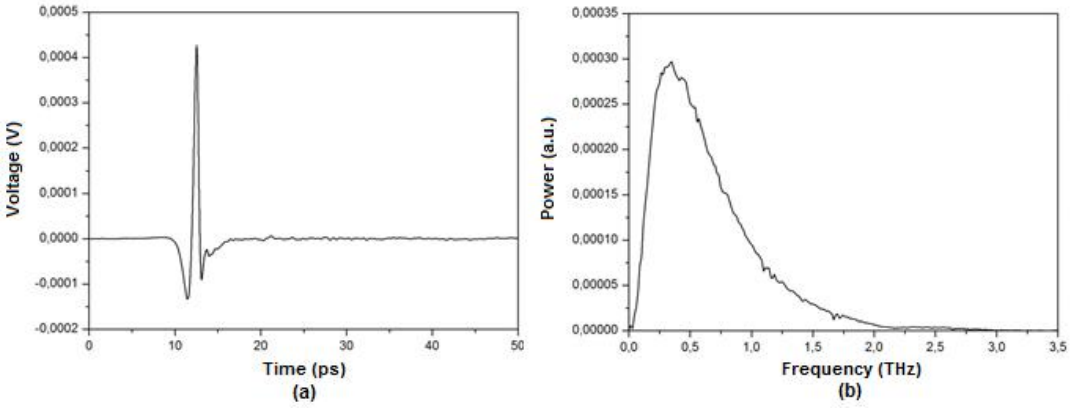

Figure 2.6: (a) THz scan of the signal in time domain and (b) power spectrum of the signal in frequency domain

2.1.2 THz Detection with Electro-Optic Sampling

Electro-optic sampling is the reverse of the optical rectification. Both techniques are described by the Pockels Effect that was mentioned in Section 1.3. In 1906 the change over the refractive index with respect to the applied electric field strength is described as Pockels Effect by Friedrich Pockels [25].

The most important factor for an efficient detection is the phase matching between the group velocity of the probe pulse, and the phase velocity of the THz wave. More efficient generation is achieved with greater interaction between optical and THz pulses in the electro-optic medium which is provided by phase matching [33].

ZnTe crystal is one of the most common electro-optic mediums in the THz-TDS systems. Because of the high sensitivity of ZnTe near 2 THz and a transverse-optical- (TO) phonon resonance at 5.3 THz this crystal is convenient for lower frequencies. GaAs and GaP are some of the birefringent crystals that should be preferred at higher frequencies [34]. Since there are options for low and high frequencies, the limits of the optical bandwidth are eliminated for the measurements performed with electro-optic sampling [35]. For this work the frequency range of ZnTe crystal was more suitable.

After the electro-optic medium a quarter wave plate is used for the compensation of the equilibrium birefringence. Circular polarized beam is obtained after the quarter wave plate for the probe pulse without THz signal and with a Wollaston prism the beam is divided into two separate polarization states; s- and p-polarization. Magnitude of these two signals is measured with a balanced photodetector.

In case of the mismatching due to the circular polarization (x=y) output of the detector is zero, as given in Fig.2.7 (a). With the help of this case, the detected electric field of the probe beam is calibrated and the angle of the quarter wave plate is fixed at the point that the polarization of the probe pulse is circular (x-y=0). On the other hand, circular polarization of the probe beam transforms to elliptical polarization (xy) with the interaction of the THz signal and non-

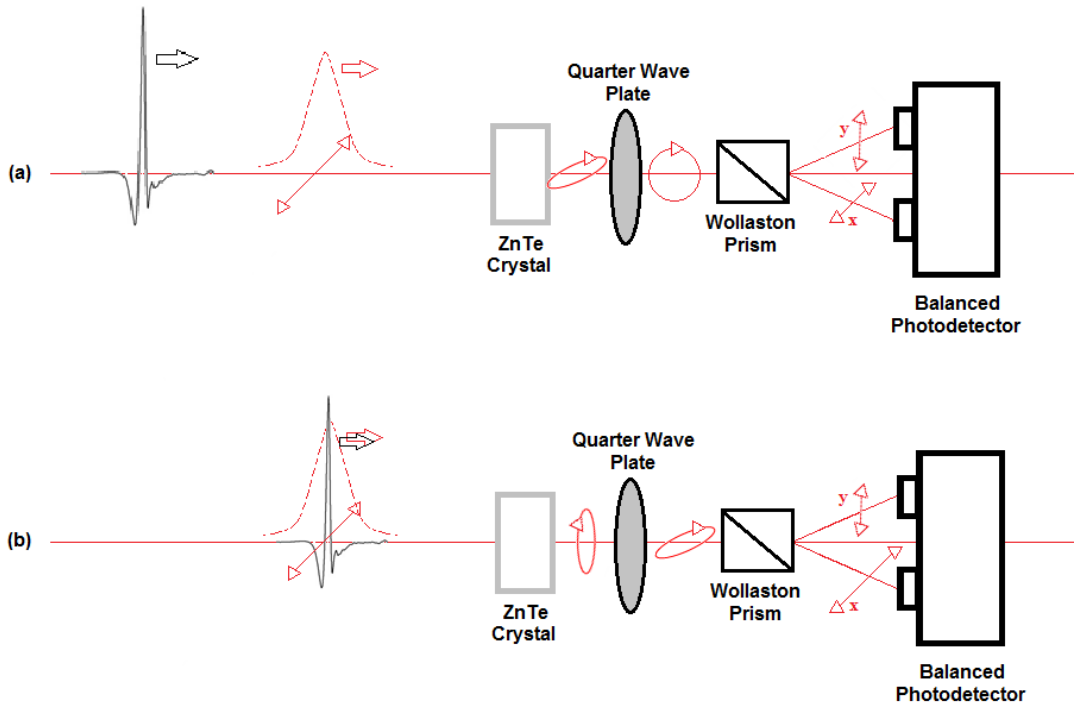

Figure 2.7: (a) Before THz signal (b) At the peak of THz signal; the pulse widths are not scaled.

zero output from the balanced photodetector is obtained, as given in Fig.2.7 (b). The calibration of the measured electric field of the THz pulse is performed to maximize the signal by changing the angle of ZnTe crystal.

2.2 THz Time Domain Spectrometer

Biological, chemical, semi-conductor, nanomaterial and metamaterial measurements have been performed with THz Time Domain Spectrometer in THz Research Laboratory, Department of Physics, METU.

A mode-locked Ti:Sapphire (Ti:Al_2O_3)laser with 800nm central wavelength, 350mW average power, 75MHz repetition rate and 17fs pulse duration is used as a source for the system. The position of the laser in the system was shown in Fig.2.8.

Output of the laser is divided into generation and detection arms by a beam

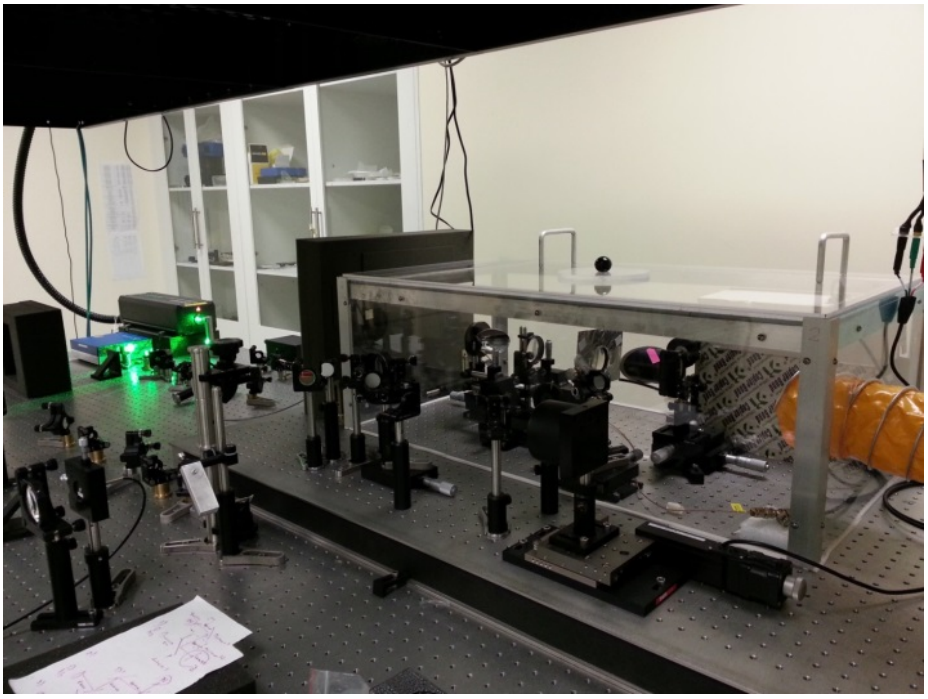

Figure 2.8: THz Time-Domain Spectrometer

splitter with a 95:5 transmission ratio. Since the requirement of power for the generation arm is much higher than the detection arm, the transmitted beam goes through the generation arm and the reflected beam goes through the detection arm. System details are given in Fig. 2.9 schematically.

The beam focuses on the semi-conductor chip of the interdigital photoconductive antenna at the generation arm. There is a connection between the antenna and the function generator that modulates it with square waves bias of +/-10V at 1kHz. Then, THz generation occurs with the focalization of the beam onto the chip. With the help of the silicon lens of the antenna, THz waves scatter through the off-axis parabolic mirror, as the antenna is placed at the focus of the off-axis parabolic mirror that collimates THz wave in Fig. 2.10(a). To increase the sample-THz interaction, the collimated THz wave is focused onto the sample using a TPX lens (D=50mm, F2), which is transparent in THz range. After focusing the spot size of the THz wave was measured as 5mm.

Another TPX lens, with the same properties of the previous lens, is used to collimate the wave through the second off-axis parabolic mirror following the

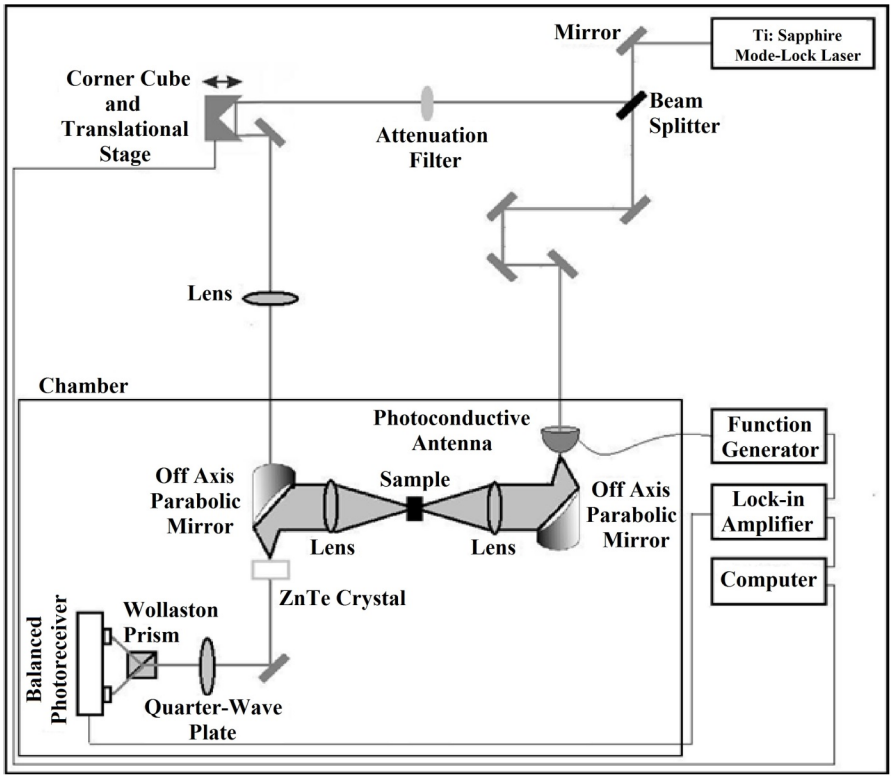

Figure 2.9: Schematic drawing of the system

sample. Then, the mirror focuses the wave onto the ZnTe crystal that is at the focus of it. The position of the crystal was given in Fig. 2.10(b).

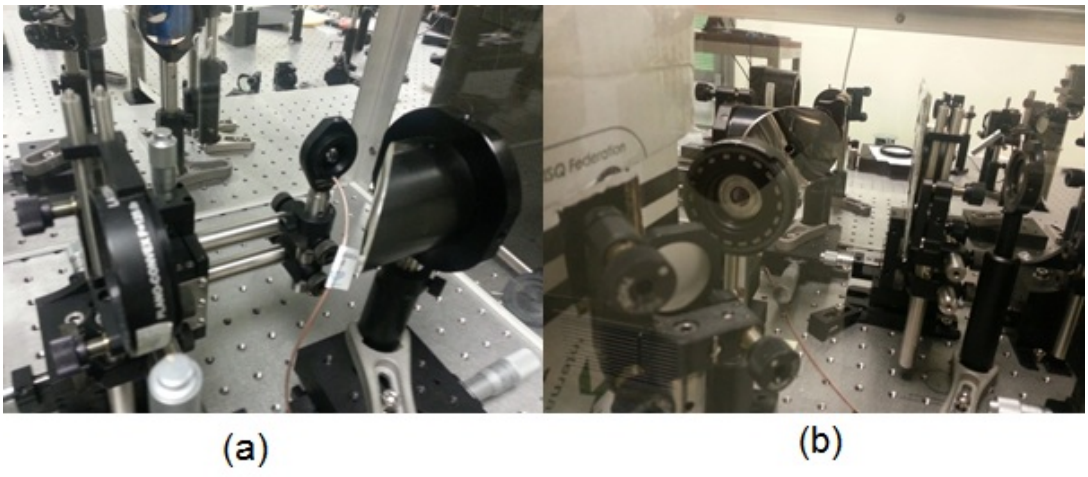

Figure 2.10: Position of (a) the antenna and (b) the ZnTe crystal at the focus of the off-axis parabolic mirror

The aim of the attenuation filter is to protect the detector from saturation by

decreasing the power in the detection arm. The beam with the sufficient power is sent to a cubic mirror that is placed on a translational stage controlled by a computer.

Afterward scanning the THz waveform through the sample becomes possible with the mobility of the translational stage. After the reflections in the cubic mirror, beam focuses with a lens onto the ZnTe crystal. By the way for electro-optic sampling with ZnTe detection crystal path lengths of the detection and generation arms have to be equal. During the scanning of the THz the pulse is observed at the point where both arms are equalized.

A quarter wave plate to control the polarization for elliptical or circular polarization and a Wollaston prism to divide the beam in to its horizontal and vertical polarizations follow the ZnTe crystal in the system. After all, divided beams reach to the balanced photodetector that is connected to a lock-in amplifier to extract the signal. Since the detector signal is small lock-in detection gives accurate results. Output of amplifier and modulation conditions of function generator (square waves bias of +/-10V at 1kHz.) are sent to the computer and supported with LabVIEW software.

For optimization of the measurements whole system was closed with a plexiglass box that blocks the air stream and provide opportunity to purge the system. Because of high absorption rates of water by THz waves system is purged with dry Nitrogen and the water absorption features at 0.38THz, 0.44THz, 0.56THz, 0.75THz, 0.99THz, 1.10THz, 1.16THz, 1.21THz and, 1.41THz are eliminated [36,37]. Elimination of these features increases the precision of the measurement.

2.2.1 Data Gathering

Balanced photodetector is directly connected to the lock-in amplifier and by changing the arrival time of the probe pulse with 10m step sizes the waveform of the THz pulse is scanned in the time domain. The LabVIEW software, which is used for the data acquisition from the lock-in amplifier, also controls the translational stage. Graphical-User-Interface of the software is shown in Fig.

2.11. The change of the THz signal in the time domain and the position of the translational stage can be observed during the measurement. Besides, at the end of the measurement the signal in the time domain transforms through the frequency domain as power spectrum and it is given with another graph.

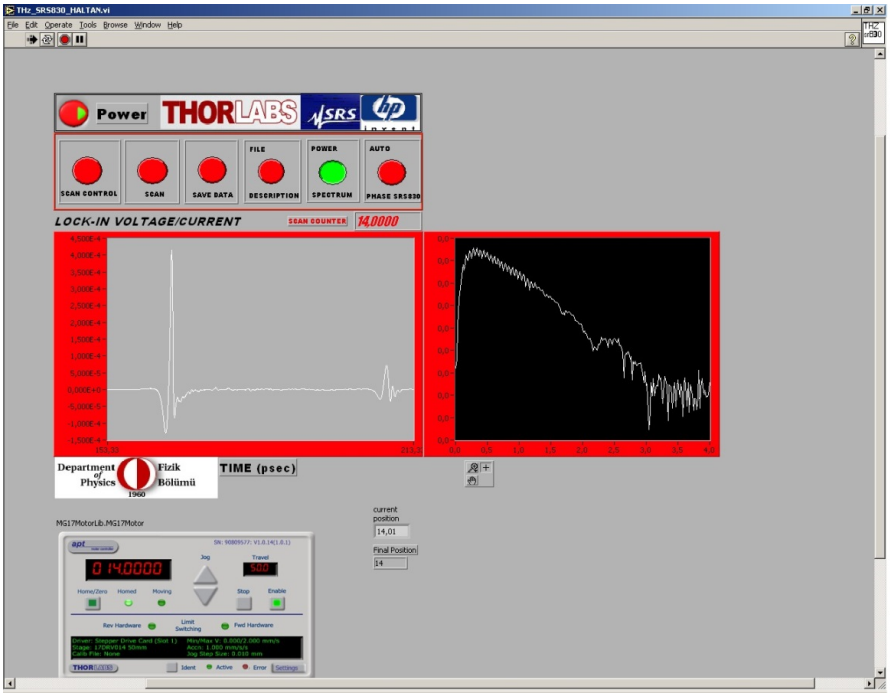

Figure 2.11: Graphical-User-Interface of the Labview software that enables the data gathering and the instrument control

The time constant of the lock-in amplifier is set to 300ms and with reference to this value the period of the 10 μmstep size is preferred as 600ms. By slowly varying the delay time of the probe pulse data points of the measurement is increased and averaging over many pulses results with higher signal-to-noise ratio and sensitivity.

2.3 Data Analysis Techniques

Time-domain THz waveforms with and without the sample requires an analysis method to create consistent inferences. Comparison of the measurements in time and frequency domain enables the direct calculations of material parameters like refractive index and absorption coefficient. One of the important variables in

these calculations is the thickness of the sample that has direct effect on the absorption ratio and time delay of the signal [38].

Complex refractive index,$\widetilde{n}$, $involves both the real part as refractive index of the material$,$n_r$, and the imaginary part as extinction coefficient, κ. Imaginary part of the complex refractive index is used for the calculations of dielectric function and conductivity that explains the attenuation through the material [39].

$$\widetilde{n} = n_r + i\kappa \tag{2.1}$$

In this work only real part of the refractive index, which can be calculated from the data gathered in both time and frequency domain, is analyzed. In Eq. 2.2, c is the speed of light, Δt is the time delay of the THz signal and, d is the thickness of the sample. (c Δt) explains the motion of light in free space (n=1) as distance and the ratio of this distance to the thickness of the sample gives the difference between the refractive index of the material and the free space. So, with the multiplication of the difference and the free space's refractive index resulted with the refractive index of the material [39].

$$n_r = 1 + (c\Delta t)/d \tag{2.2}$$

To calculate the refractive index from frequency domain data time shift rewritten with phase shift, $\Delta\phi$, and, frequency, ν in Eq.2.3.

$$\Delta t = \Delta\phi/2\pi\nu \tag{2.3}$$

By substitution of Eq.2.3 into Eq.2.2 frequency dependent refractive index formula is obtained.

$$n = 1 + (c\Delta\phi)/(2\pi\nu d) \tag{2.4}$$

Intensity of the incident beam is decreased through the material. While absorption and transmission are the reasons of the attenuation of the optical power, reflections and scattering are negligible. T is transmittance through the sample, I is the intensity of the pulse after the transmission and, I_0 is the intensity of incident pulse in Eq. 2.5.

$$T = I/I_0 \tag{2.5}$$

Intensity of the incident beam changes through the material as an exponential function and the number of photons absorbed by the material per unit thickness

[cm-1] changes exponentially with the thickness of the sample. The relationship between the variables are given in Eq. 2.6 where α is the absorption coefficient.

$$I/I_0 = e^{-\alpha d} \tag{2.6}$$

In Eq.2.7 absorption coefficient is defined as thickness and transmittance with the reference of the Eq. 2.6 [39].

$$\alpha = (-1/d)ln(T) \tag{2.7}$$

With the help of these formulas refractive index and absorption coefficient are directly calculated by data analysis software. In this work, the analysis is performed with Origin and PKGraph.

2.3.1 Analysis Using Origin

Origin is scientific graphing and data analysis software for wide area of usage. First step of the analysis is optimization of the data for Fast Fourier Transform (FFT). If thereare any reflections from the beam splitter after the THz signal, the data points after the beginning of the reflection are not included to the analysis. Due to the fact that the mathematical definition of the FFT depends on the base 2 logarithm, total number of data points should be equal to 2n, where n is an integer. For example, 1024 data point is used in this work.

After FFT, power and phase information in frequency domain is obtained. To calculate the transmittance the definition of the intensity in terms of power and area is used, given in Eq. 2.8 where P is the power of the transmitted beam, P_0 is the power of the incident beam, and A is the area.

$$T = I/I_0 = (PA)/(P_0A) = P/P_0 \tag{2.8}$$

Eq. 2.4 and Eq. 2.7 are inserted into the software as formulas and and P/P_0 are defined as columns that show the changes in frequency domain.

2.3.2 Analysis Using PKGraph

PKGraph is the data analysis software for THz spectroscopy that was provided by Center for Terahertz Research, Rensselaer Polytechnic Institute. With PK-

Graph reflections can be eliminated with the summation of the reverse reflection signal. This tool prevents the loss of data points that occurs for the analysis performed with Origin. All formulas related with these calculations are available in the software that could be evaluated as an improvement for the error rate and consistency of the analysis.

Transmission lines of the air measurements with 29% and 4% of humidity are compared and the absorption features of water are observed using both PKGraph and Origin. The one at 0.56THz is given in Fig. 2.12; the dept of the absorption is almost the same for both analyses and maximum absorption is observed at the same frequency, 0.56THz. PKGraph and Origin could be used as a verification method for each other.

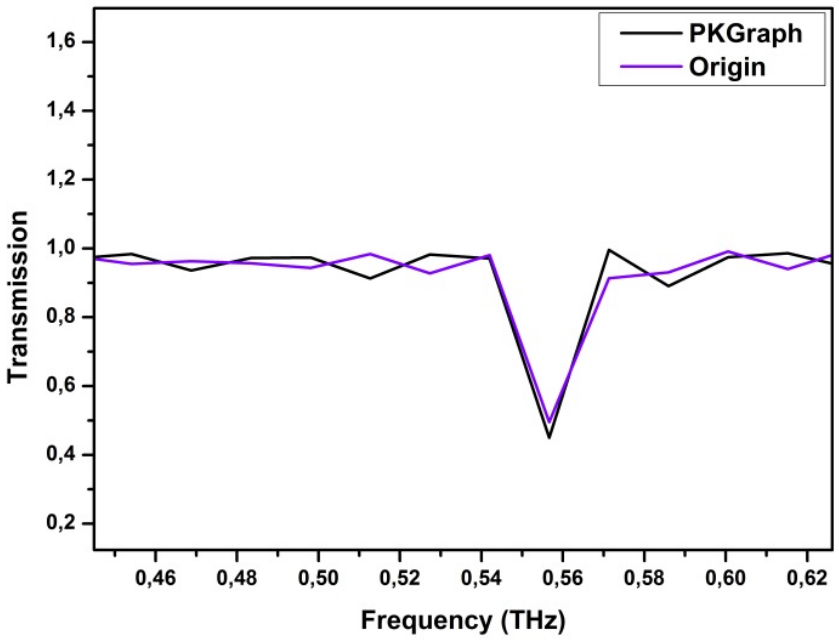

Figure 2.12: Comparison of PKGraph and Origin with respect to the absorption feature of water molecules at 0.56THz

CHAPTER 3

BIOLOGICAL MEASUREMENTS

Interdisciplinary works in spectroscopy have led to new research topics in the recent years. For this work, collaborations with Faculties of Dentistry, Ankara University, Plastic and Reconstructive Surgery, GATA and, Department of Biology, METU were done for each biological measurement. Performed biological measurements are classified in three different categories: hard tissue, soft tissue and, amino-acid measurements.

3.1 Hard Tissue Measurements: Tooth

Human tooth consists of four main parts, namely: enamel, dentin, cementum, and pulp, as given in Fig. 3.1. The materials that comprise these parts are different, and that causes the difference between the properties of these tissues. Characteristics of the parts are directly related with the health level of the tooth [40].

In this work there were two main groups, namely; primary and adult tooth samples. Primary teeth are temporary structures in a child's mouth and replaced by the permanent ones; adult teeth. The difference between their morphological features can be observed without any equipment but the histological and mineral content differences should be analyzed with further thoughts. Enamel thickness, pulp chamber size, and recovery ratio of the dentin are some examples of the characteristics that should be compared for primary and adult teeth with more special measurement techniques [41]. Four primary and four adult extracted

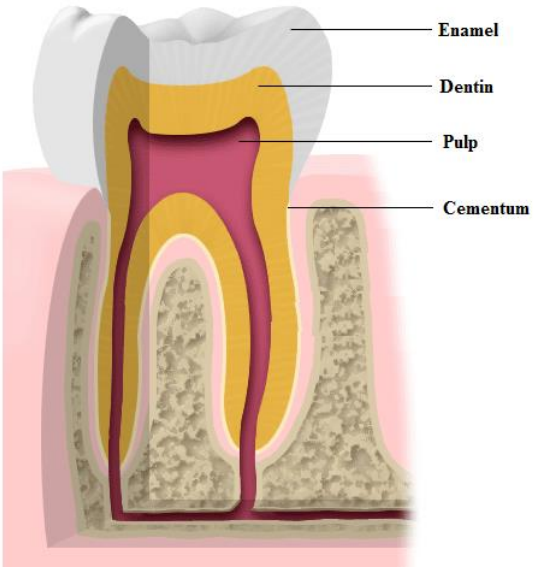

Figure 3.1: Main parts of a tooth

human teeth, Fig.3.2 (a) and (b), were measured with the THz-TDS system.

Human tooth samples were obtained from Ankara University, The Faculty of Dentistry. After teeth were pulled, they were stored in serum fluid at room temperature until each tooth was serially sectioned mesiodistally in parallel to the long axis by using a water cooled diamond saw at low speed. The samples were prepared for transmission measurements where each tooth was thinly sliced along the long axis so that the THz radiation could probe the layered structure of the sample.

THz wave is focused on a 5mm diameter area of the samples which was circled in red in Fig.3.2 (a) and (b) for each sample. Primary and adult tooth samples were classified in their own as healthy samples and samples with caries (tooth decay) with reference to the areas. This categorization was resulted in four types of samples; primary-healthy teeth, primary-teeth with caries, adult- healthy teeth and adult-teeth with caries.

In vivo conditions were also evaluated by the comparison of wet and dry samples. Dentin tissue includes microscopic channels that are named dentinal tubules. These structures lie from dentin/pulp interface to enamel and contain cellular structure and fluid [42]. The effects of the fluid in dentinal tubules were observed

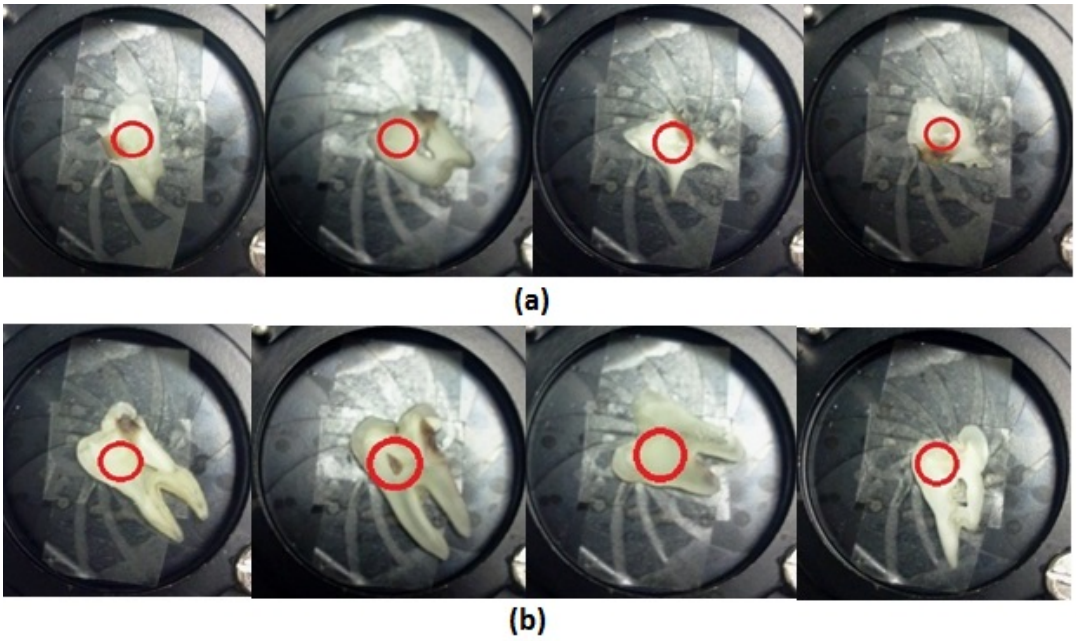

Figure 3.2: (a) Primary Tooth Samples; Sample 1, 2, 3, and 4 (b) Adult Tooth Samples; Sample 5, 6, 7, and 8

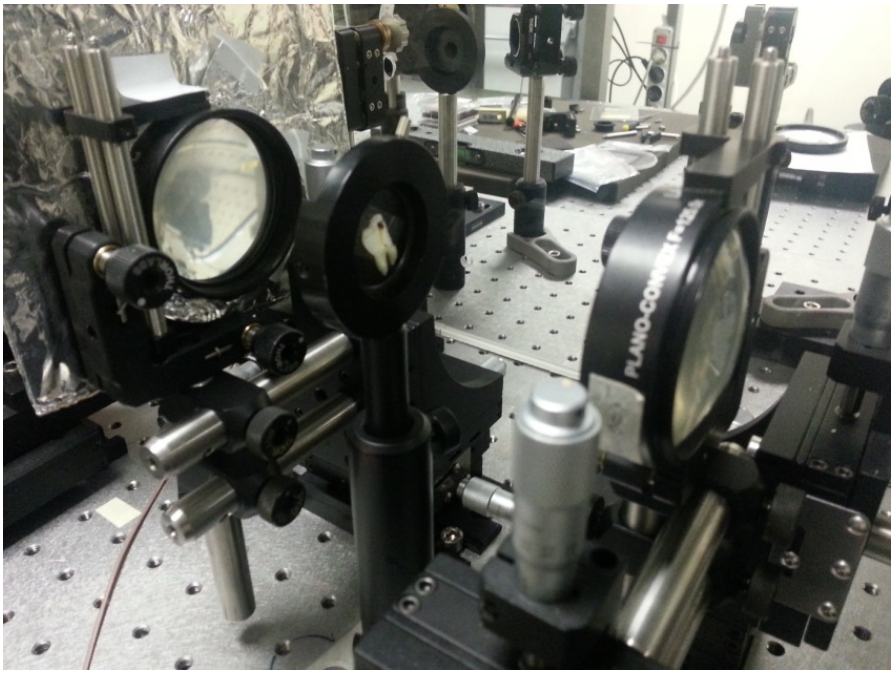

Figure 3.3: Position of a tooth sample in the THz-TDS system

with two types of measurements. Initially, right after the slicing process the samples were stored in deionized water instead of serum fluid and measured in the wet state. Secondly, after drying them for a few days they were measured in the dry state. Deionized water was used for creating a wet environment such as the mouth.

3.1.1 THz-TDS Measurements

Analysis of wet and dry state measurements was the starting point of this work. The refractive index and power absorption of the samples were investigated in both states. THz time-domain scans of a healthy primary tooth sample (Sample 4) in wet and dry states are given in Fig.3.4.

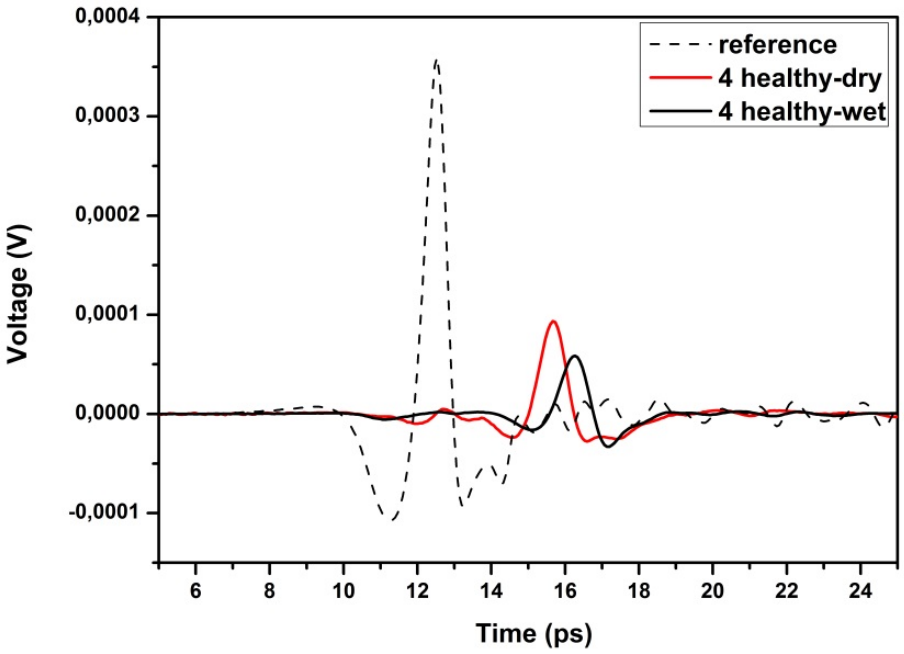

Figure 3.4: THz scan of a primary tooth sample in wet and dry states

Refractive indices of dry and wet samples were approximately 2.3 and 2.0, respectively. In Fig.3.5 the slopes of the refractive index lines are similar. On the other hand, the magnitude difference of the lines is because of the increase of the refractive index after the sample was dried out. The reason of the change is

the lower refractive index of water than tooth sample.

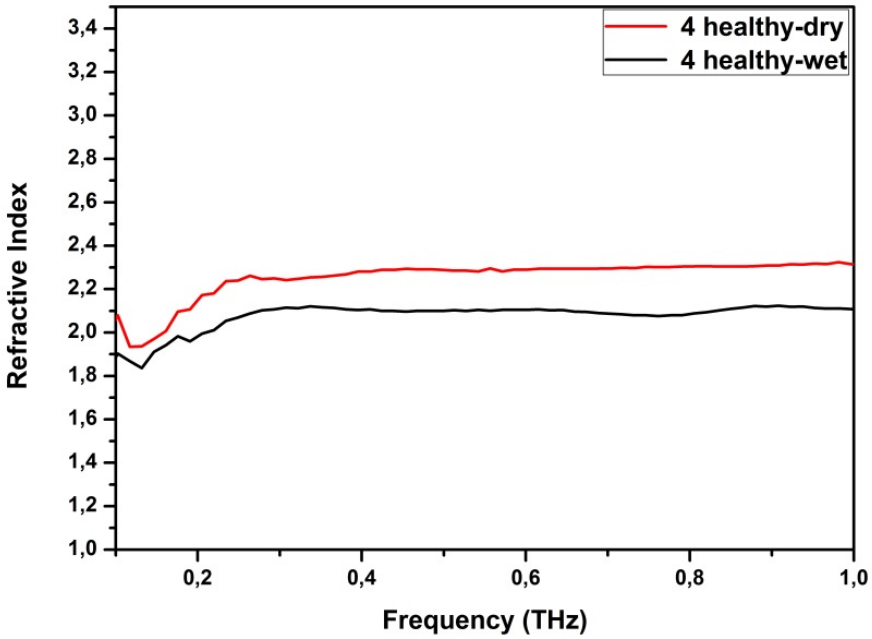

Figure 3.5: Refractive indices of a sample in wet and dry state

By reason of the absorption by water content, the power absorption of wet sample has larger absorption coefficient than dry one. Due to the high absorption rate of water in THz range it was an expected result.

In brief wet samples have lower refractive index and higher power absorption compared to dry samples which is expected because of the liquid's physical properties. As a result of the conclusion for wet and dry states, other sample groups would be analyzed only in wet state to optimize the environmental conditions for in vivo tooth imaging.

Four primary (Sample 1, 2, 3, and 4) and four adult (Sample 5, 6, 7, and 8) tooth samples, Fig.3.2 and Fig.**??**, were labeled as either having caries (decay) or healty (intact). Intact samples has a smooter surface than the ones with caries. On the other hand, samples with caries have irregular surfaces that can cause scattering. THz scans of the all samples and the reference was given in Fig.3.7. Primary teeh samples and adult tooth samples are measeured in the

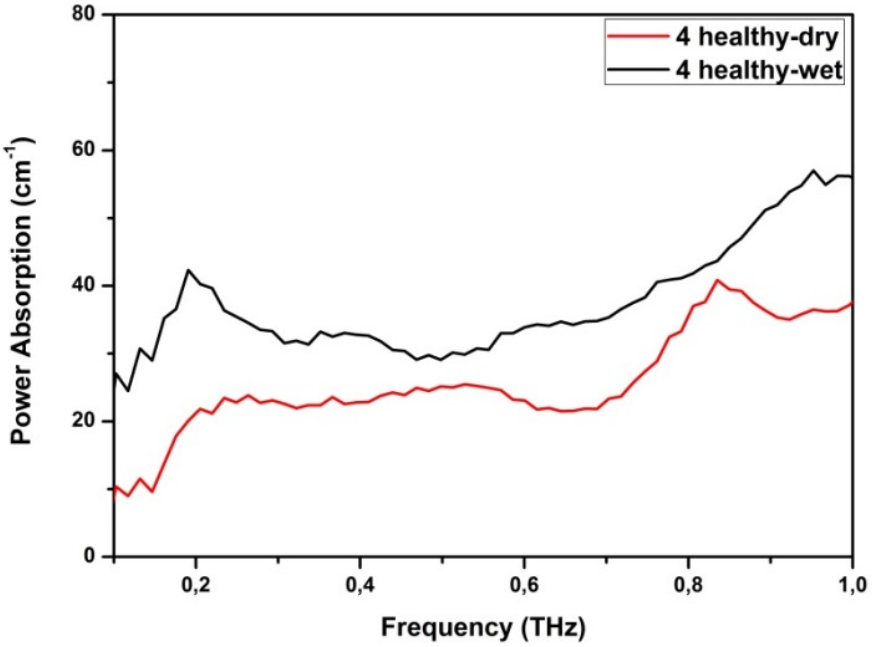

Figure 3.6: Power absorptions of a sample in wet and dry state

order of ranges 13-23ps and 15-25ps. The structural difference of these samples is the main reason for the shift of the range. The magnified scans of primary and adult tooth samples in time domain are shown in Fig.3.8 (a) and (b). In Fig. [?] and [?] double peaks were observed because of the heterogeneous structure of tooth samples, such as; mixture of dentin, enamel and, pulp, and the variation of the thickness through the sample.

In Fig.3.9 the refractive indices for primary-healthy tooth samples and primary-tooth samples with caries are given. Refractive indices of primary-healthy tooth samples are higher than the primary- tooth samples with caries. Cavities and other types of deformations on the surface of the sample causes scattering from the irregularities and decreases the transmission amplitude for the sample. Scattered part of the amplitude, has no effect on time-shifting, could be observed as absorbed and the result would be higher power absorption and smaller refractive index. Normally, for healthy tooth samples flat refractive indices,like Sample 1, was expected as a result but, health status of the tooth is not the only factor that

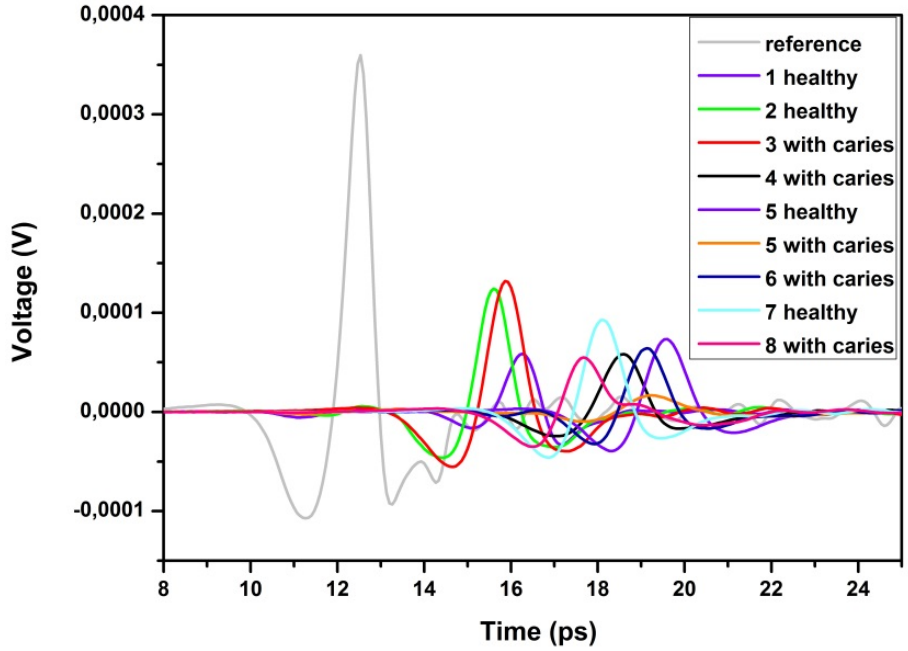

Figure 3.7: THz scan of tooth samples

effect the measurement results. Morphological Deformation and measurement of pulp part of the sample affect the ratio of THz transmission. Although there isn't any morphological deformation on Sample 2, pulp part of the sample was included the measurement. So, the decrease around 0.43THz can be explained as the effect of the pulp on measurement. Approxiamate values for Refractive indices of Sample 1,2,3, and 4 are in order of 2.53, 2.46, 2.29 and, 2.1 around 0.5THz.

The refractive indices for adult-healthy tooth samples and adult- tooth samples with caries are compared in Fig.3.10. Refractive indices of healthy samples are also higher than the ones with caries for adult tooth samples. Refractive indices of Sample 5 and 7 are flat around 2,62 and 2.55 between 0.5THz-1THz, respectively. Sample 5 and 7 have higher and smooter refractive indices of than Sample 6 and 8, that have refractive indices nearly 2.5 and 2.45 around 0.5 THz. Caries of Sample 8 is not partial like other samples. Whole measured area shows signs of structural deformation from inside of the sample; like color change and

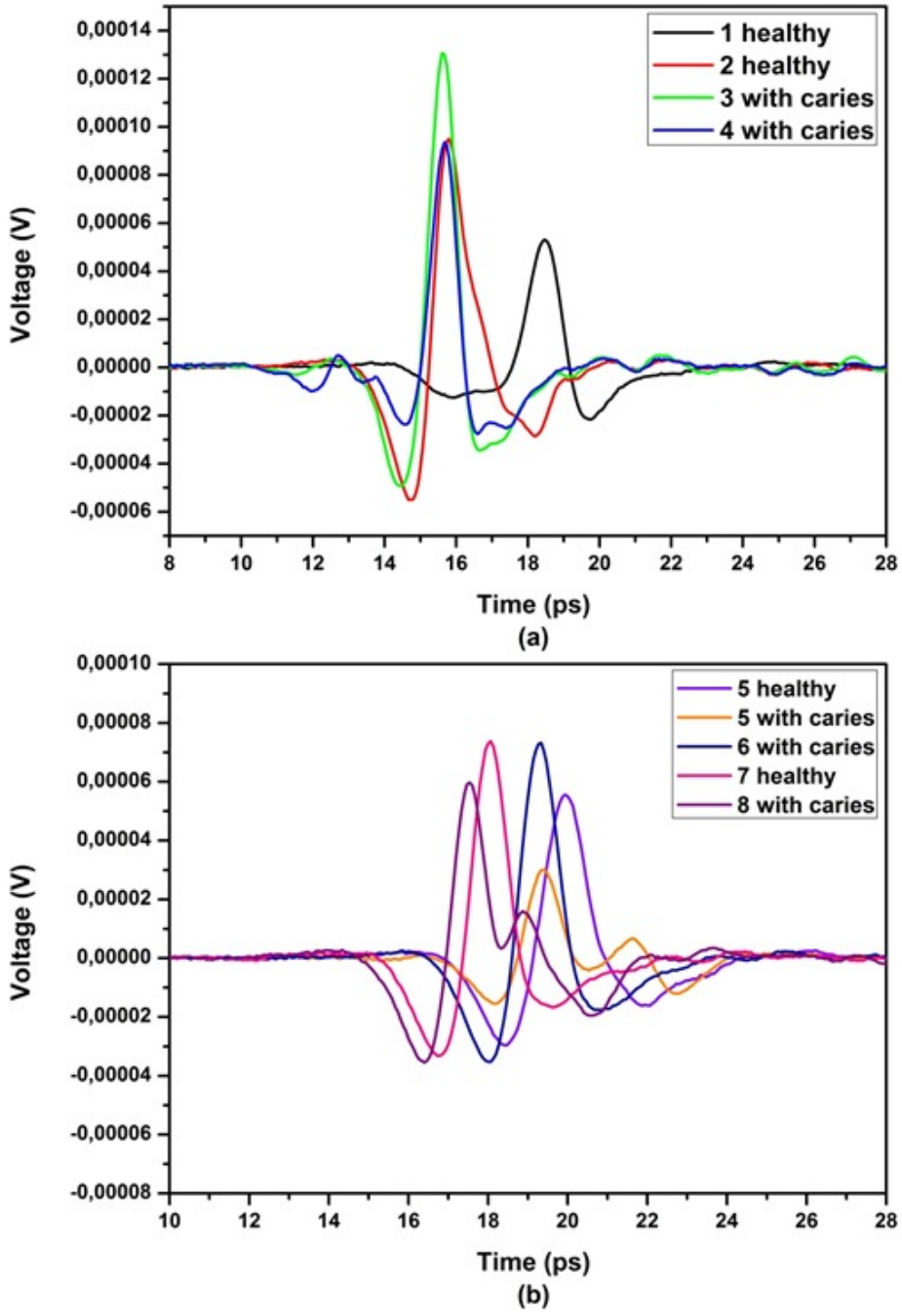

Figure 3.8: THz scan of (a) the primary tooth and (b) the adult tooth samples

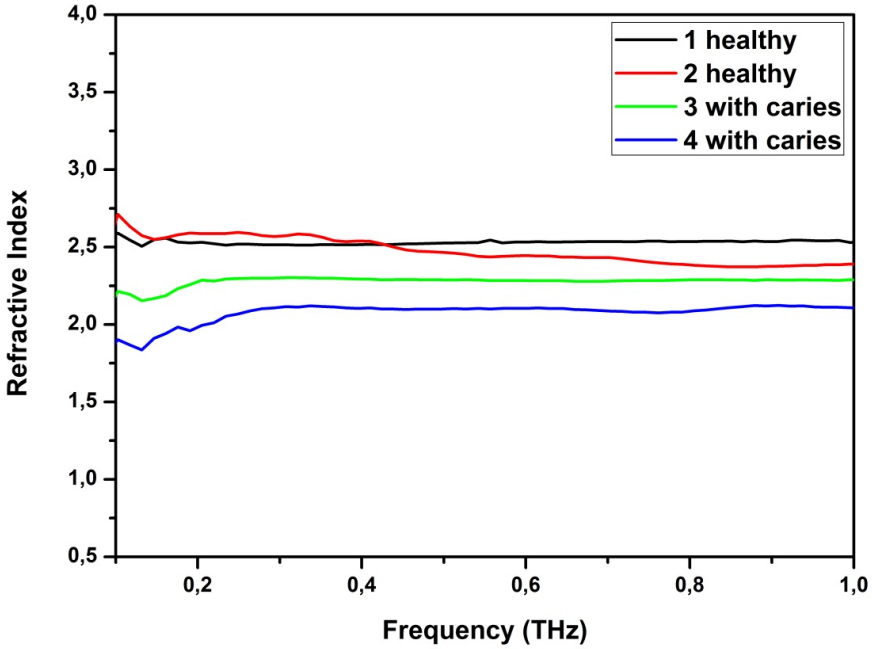

Figure 3.9: Refractive indices of the primary tooth samples

absence of cavities. Therefore the decrease around 0.3THz in Fig. 3.10 could be a clue for the deformation of Sample 8. On the other hand, the smaller refractive index of Sample 6 is the result of scattering from irregular surfaces like primary tooth samples with caries.

Primary and adult tooth samples with caries have lower refractive indices than healthy ones. The main reason of the difference is scattering from the decayed part of tooth. Furthermore, the refractive index of various healthy primary and adult teeth was measured around 2.5 with slight differences that depend on the part of tooth sample was measured like dentin, enamel or pulp.

Refractive index value of a tooth sample depends on type of the tooth, thickness, parts of tooth that were measured, health status of sample and any morphological deformation. For all of the eight samples these properties are listed in Tab.3.1 to sum up.

Power absorption of primary-healthy tooth samples and primary- tooth samples

Sample #	Type of Tooth	Thickness ±0,2 (mm)	Parts of Tooth in 5mm Diameter Area	Refractive Index	Health Status	Morphological Deformation
1	Primary	1,03	Enamel and Dentin	2,53	Healthy	Non
2	Primary	0,84	Pulp and Dentin	2,46	Healthy	Non
3	Primary	0,77	Pulp and Dentin	2,29	Caries	Cavities on both surfaces, hole at the center
4	Primary	0,88	Pulp and Dentin	2,1	Caries	Cavities on both surfaces, hole at the center
5	Adult	1,38	Pulp and Dentin	2,56	Healthy	Non
		0,79	Enamel and Dentin	2,52	Caries	Cavity on one surface
6	Adult	1,26	Pulp and Dentin	2,48	Caries	Cavity on one surface
7	Adult	1,11	Pulp and Dentin	2,52	Healthy	Non
8	Adult	1,07	Dentin	2,45	Caries	Non

Table3.1: Summary of the refractive index measurements

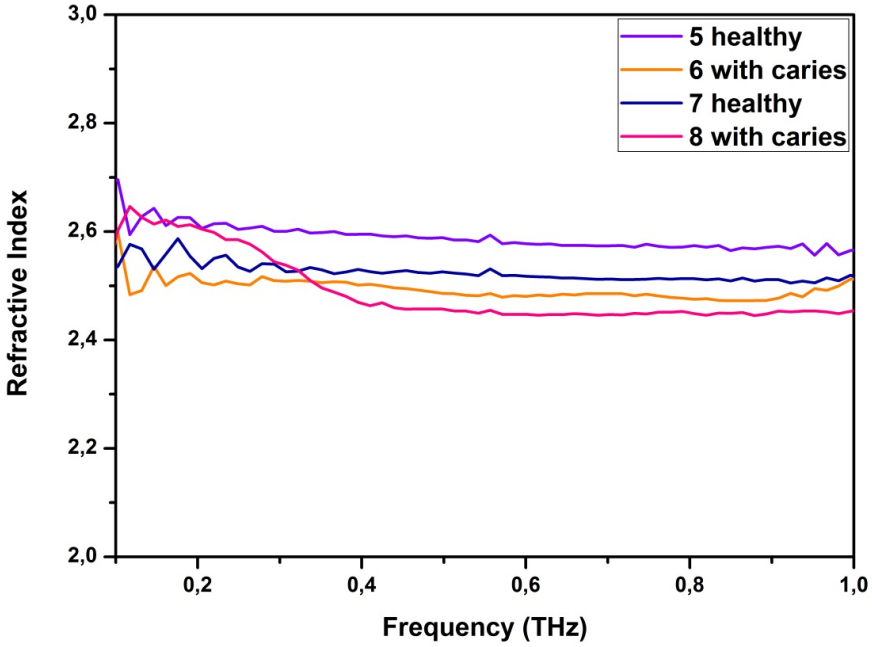

Figure 3.10: Refractive indices of the adult tooth samples

with caries are given in Fig.3.11. Between 0.1 and 0.5 THz power absorption of primary tooth samples with caries higher than primary healthy ones.

In Fig. 3.12 power absorption of adult-healthy tooth samples and adult- tooth samples with caries shows the difference between healthy and decayed tooth samples more clear than the primary tooth samples. The result is similar with primary tooth samples; between 0.1 and 0.5 THz power absorption of adult-tooth samples with caries are higher than adult-healthy ones. Afore-mentioned structural deformation of Sample 8 and the cavity at the center of the measured area of the Sample 6 is the main reasons of the higher absorption coefficients than the healthy ones.

During THz interaction of the samples, rough surfaces cause scattering that increases the power absorption that was measured [43]. Consequently, power absorption of tooth samples with caries is higher than healthy ones for both primary and adult tooth sample groups between 0.1 and 0.5 THz.

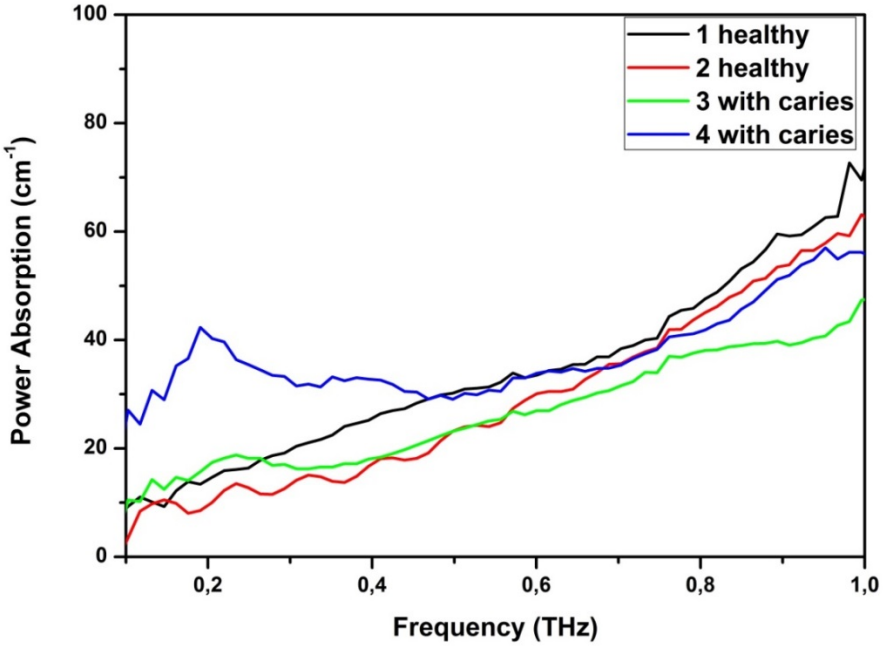

Figure 3.11: Power absorption of the primary tooth samples

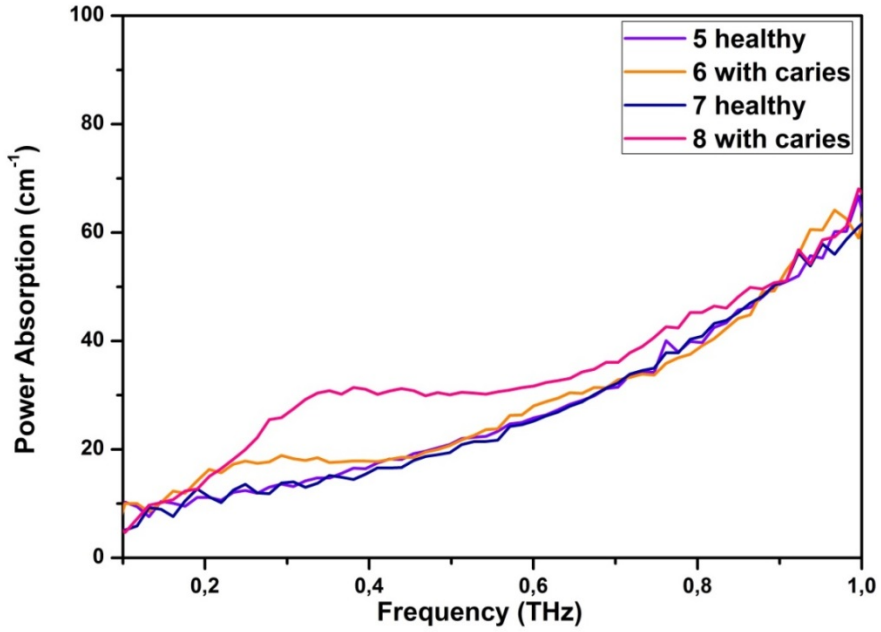

Figure 3.12: Power absorption of the adult tooth samples

Primary and adult tooth samples with caries have lower refractive indices and higher power absorption (between 0.1 and 0.5 THz) than healthy ones. The result of the sample groups were investigated for only one sample. Two different parts of an adult tooth sample (Sample 5) were measured and labeled as healthy tooth sample and tooth sample with caries, Fig.3.11 (a) and (b).

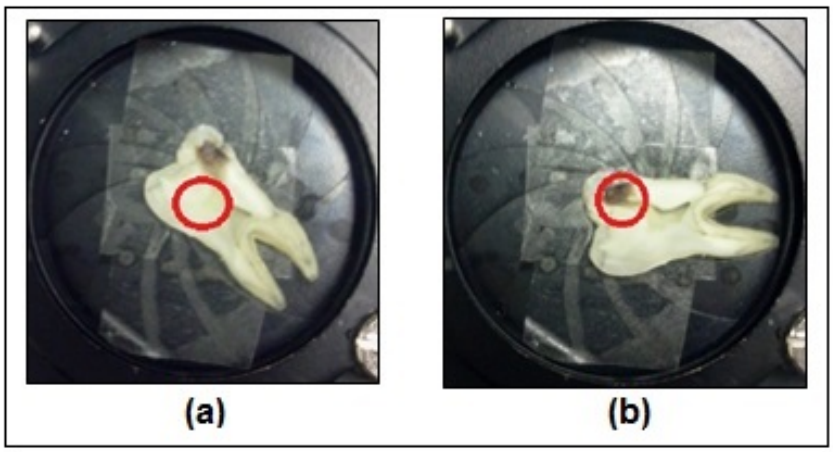

Figure 3.13: (a) Healthy area of Sample 5 (b) Area of Sample 5 with Caries

THz signals of these two parts and the reference signal are shown in Fig..3.14. Because of the scattering from the cavity, the decrease of the signal amplitude is observed. Also, the thickness of the sample decreases at the cavity part so, the signal of sample with caries is closer to the reference signal. In other words, time-shift value decreases with the reduction of the thickness.

Refractive index of healthy part of Sample 5 is higher than the one with caries. Also, healty part measurement has a flat refractive index with respect to the part with caries like previous measurements. The comparison of two parts is given in Fig.3.15.

Power absorptions of healthy part and part with caries are given in Fig.3.16. Absorption coefficient of the part with caries is higher than healthy one between 0.1 and 1THz. Health status inspection with power absorption is easier with single sample measurements compared to previous evaluations of primary and adult tooth samples.

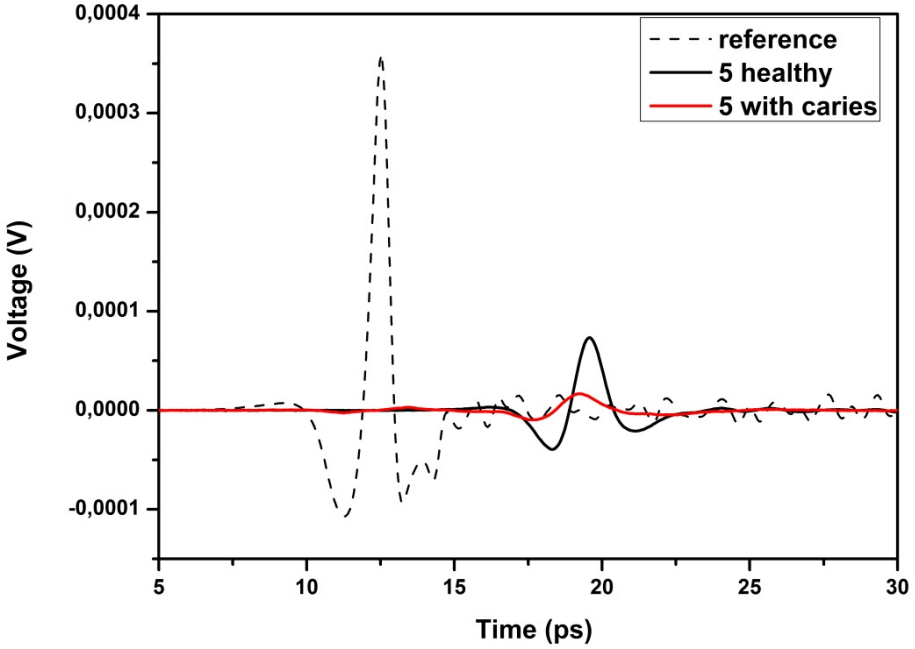

Figure 3.14: THz scans of Sample 5 for healthy part and part with caries

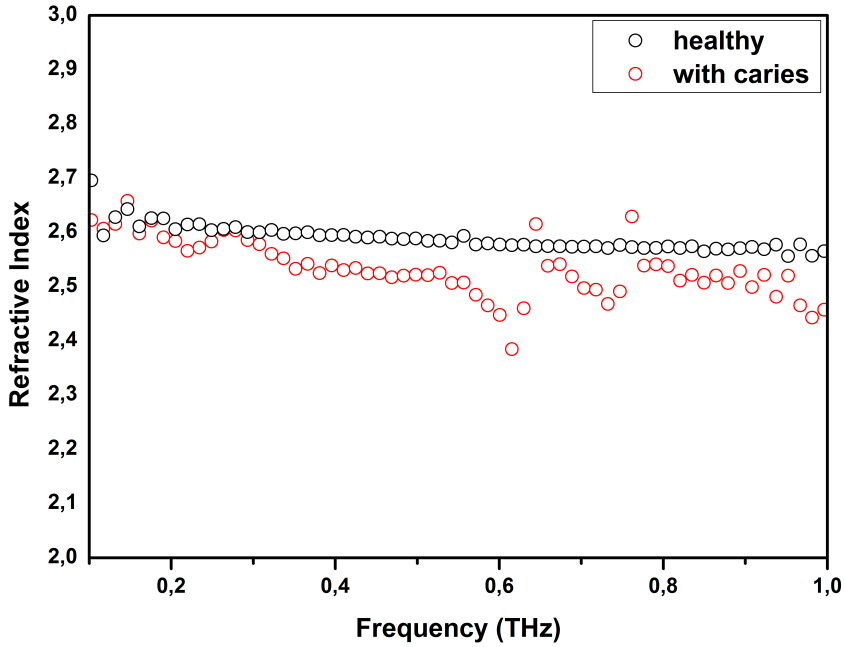

Figure 3.15: Refractive indices of healthy area and area with caries of Sample 5

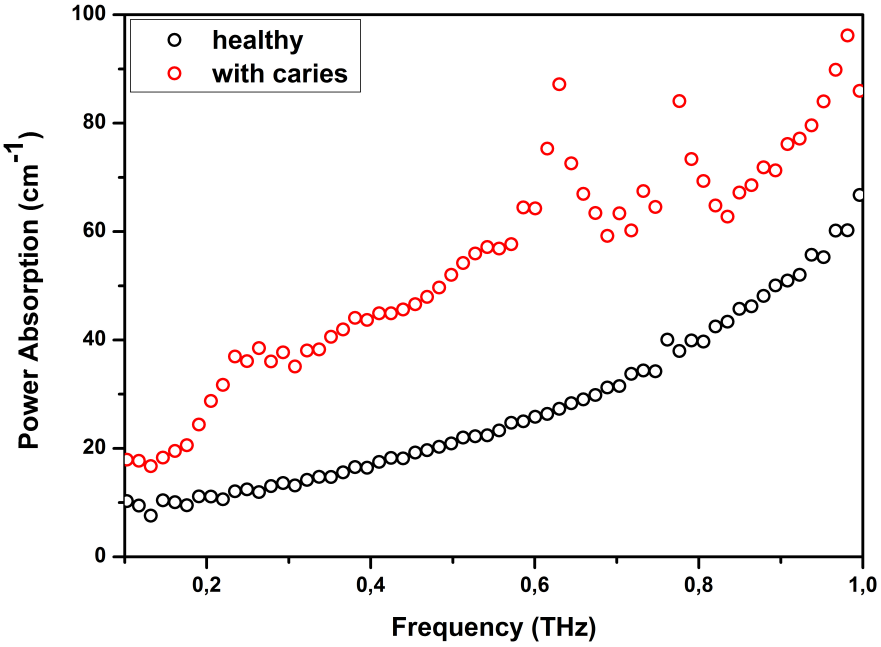

Figure 3.16: Power absorption of intact and decayed areas of Sample 5

As a result, comparison of single and multiple samples' measurements show that decayed part of a tooth sample decreases refractive index and increases power absorption between 0.1 and 0.5 THz because of scattering.

3.1.2 Results and Discussion

Terahertz studies have gained remarkable importance for several medical application areas. Research in dentistry is starting to concentrate upon these studies because of less harmless radiation level than X-ray for children and pregnant patients. THz imaging enables to have better imaging contrast with the effect of scattering [43].

The refractive index and power absorption of the tooth samples were analyzed between 0.1-1THz in the wet and dry states. These states were compared and because of the liquid, results showed clear differences on refractive index and power absorption. Wet samples have lower refractive index and higher power

absorption compared to dry samples. Heterogeneous structure of tooth samples and the variation of the thickness are some important factors that effect the measurement. Also, due to the scattering from the decayed part of the tooth, refractive indices and power absorptions of these samples indicated differences between healthy tooth and tooth with caries. Refractive index of healthy samples is higher than the one with caries and power absorption of samples with caries is higher than healthy ones between 0.1 and 0.5 THz. These results show that decayed parts of a tooth would create great imaging contrast in THz range and these techniques can be applied towards in-vivo diagnostics as an alternative to X-ray to characterize the tooth for dental surface irregularities.

3.2 Soft Tissue Measurements: Skin

In 2004 worldwide statics about the incidence of burns, that had the requirement of medical attention, was at the fourth rank in all injuries with almost 11 million people. Globally, every year 300.000 of these incidences are resulted with death [44].

There are clinically three classifications of burn injuries with respect to the depth, namely; first degree burn, second degree burn and third degree burn. The first degree burns (superficial burns) are the injuries, which have a spontaneous healing process, with the limited depth in epidermis layer of the skin. When this type of burns heals without any medical care, usually there won't be any scars. The depth of the second degree burns (partial thickness burns) can change and it involves the entire epidermis and some part of the dermis. The healing time is directly related with the depth of the injury; it may be superficial partial thickness or deep partial thickness burns. Generally, treatment of second degree burns depends on careful monitoring to prevent infection, but it may require surgical intervention for some of deep partial thickness burns. The third degree burns cannot heal without surgical excision and skin grafting. The depth of the injury comprises the whole skin layers: epidermis, dermis and, stratum corneum [45–47]. Depths of the burn injury types are given in Fig. 3.17.

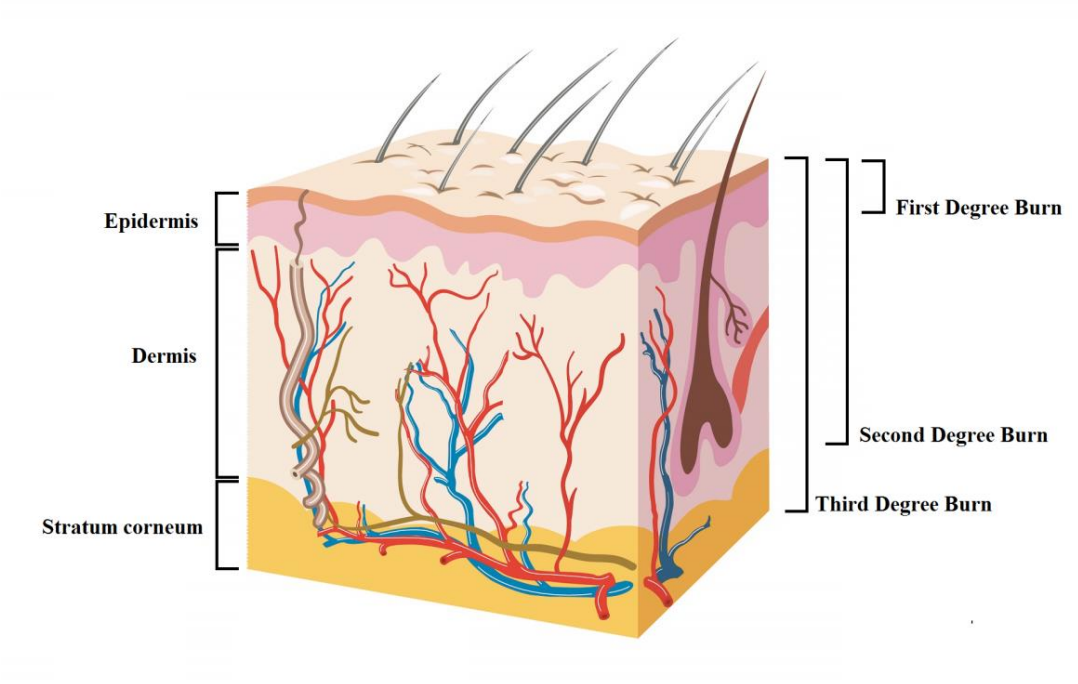

Figure 3.17: Structure of the skin and types of burn injuries [2]]

Management of burn injuries depends on the classification of burn injuries according to the damaged layers of skin. The classification result of the early post injury assessment is the most critical point about the decision method of the treatment. Ultimate spontaneous healing or surgical treatment may be the preferred method. Decision of the treatment specifies the healing period and ultimate result of the injury. Symptoms of first and third degree burns are clear to characterize. However, only around 64-70% of initial assessments in clinics are accurate for second degree burns [47, 48]]. With the accurate assessment the healing process gives results with shorter recovery period and minimum scar formation. Therefore, waste of time and money is prevented for patient [49].

Different kind of diagnose techniques have been compared in accordance with sufficient specificity and sensitivity for the early post injury assessment of burn injuries. These techniques are multispectral photo acoustic, laser Doppler imaging (LDI), optical reflection imaging, Indocyanine green dye fluorescence techniques, Nuclear Magnetic Resonance (NMR) imaging, ultrasonography, contact dielectric measurement at radio frequencies, Polarization-Sensitive Optical Co-

herence Tomography (PS-OCT), and near infrared spectroscopy. Some of them give promising results but, highest contrast level for as early as 1-h post burn has been observed with THz medical imaging [45, 48, 49].

Local water concentration of the burned tissue is directly related with the post-injury inflammatory response [49]. The high sensitivity to water is the most remarkable property of THz imaging for imaging the gradient in water content [49, 50]. Increase of the water concentration has been observed with THz spectroscopy during the inflammatory response [48, 49]. During previous researches different kind of animal tissues has been used; chicken muscle, frozen porcine skin, and rat skin. These researches get the same result; local water concentration changes at burned sections of samples and these parts have lower THz reflectivity with respect to healthy samples [45, 49]. Also, THz waves are sensitive to the density of the skin structures that can be differentiated between viable and unviable tissue with THz imaging [48, 49]. Primary contrast mechanism of THz imaging is the difference of water content in burned and unburned tissues. In addition, reduction in the discrete normal skin structures; microvasculature, sweat glands, and hair follicles can be used as a contrast mechanism in THz imaging [48, 50].

In this work burned rat skin was investigated with THz Time-Domain Spectrometer. Sample was procured from GATA, Department of Plastic and Reconstructive Surgery. Measurements were done in transmission mode and burned rat skin measured with and without water content.

3.2.1 THz-TDS Measurements

Burned skin sample was placed on a glass plate (slide) then, a holder with 8mm spot diameter was used to stabilize the slide. Thicknesses of the sample and the slide were 1.19mm and 0.17mm, respectively. Reference measurements were the measurements with only the holder and holder with slide. Next measurement was with burned rat skin on the slide. After around 0,5ml of deionized water was dropped on the slide, the burned rat skin sample was fixed on it again and final measurement was performed with this mergence.

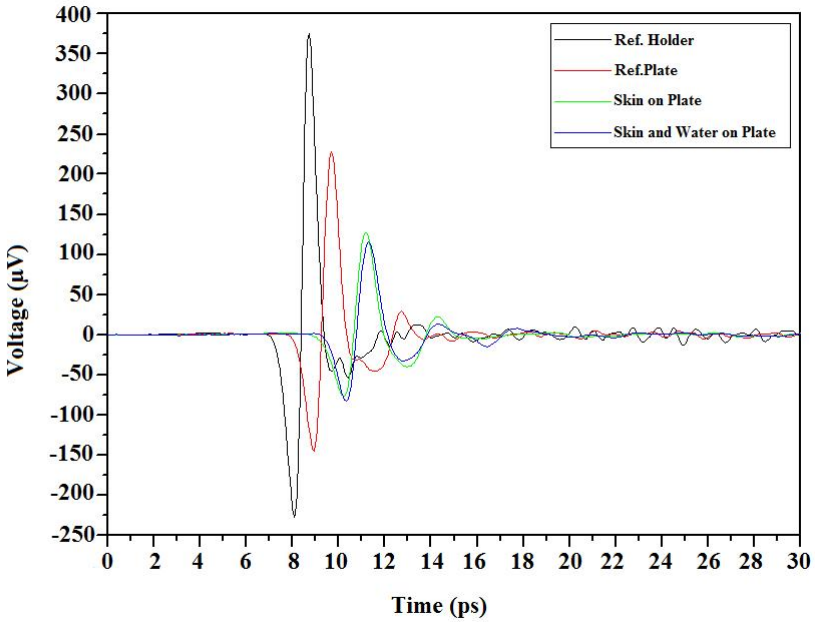

Figure 3.18: THz scans of the reference and sample measurements

In Fig.3.18 transmission of the THz pulse through holder, holder with slide, burned skin rat on slide and, burned skin rat and water on slide was given. The shift on the time domain and the decrease on THz signal were clearly seen with the comparison of the THz scans of "Skin on Plate" and "Skin and Water and Plate" in Fig.3.18 because of the water content.

Refractive index of the glass plate was found around 2.6 and the difference between the refractive indices of "Skin on Plate" and "Skin and Water on Plate" is hard to observe because of the larger refractive index of glass.

Power absorptions of the samples are given in Fig. 3.19. The glass plate has a large absorption coefficient compared to skin and water. For more precise measurements plastic or quartz plates could be better instead of glass. Around 0.5THz distribution of the water is disordered because of the burn. Power absorption of "Burned Skin and Water" is much larger than the absorption coefficient of"Burned Skin" from 0.6-1THz.

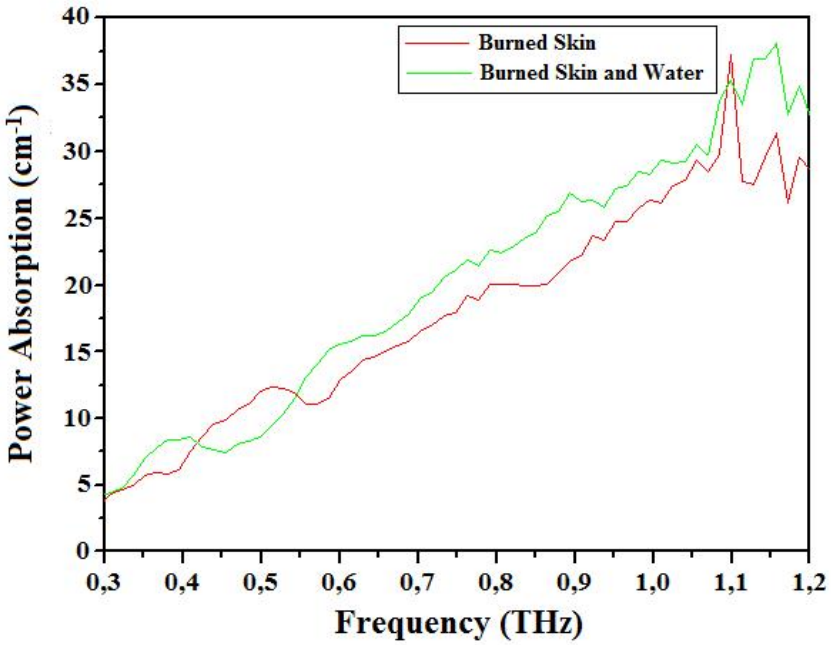

Figure 3.19: Power absorption of the burned rat skin sample and water content

3.2.2 Results and Discussion

Many biological applications of THz technology depend on the tissues' water content. High sensitivity to water absorption is a remarkable property of THz that is an advantage for imaging of burn injuries. This provides a sensitive signal contrast that makes THz imaging an effective technique with higher contrast level than the other imaging methodologies [48].

The penetration of THz waves through nearly 1.2mm skin layer and 0.5ml water content underneath the skin sample was measured. There wasn't a clear difference between the refractive indices of the samples, so they are not given in this work. However, the absorption coefficient shows great difference between the two samples in the range of 0.6-1THz. The results of the previous researches with burned rat skin model are consistent with the results that are found from the experiments about the frequency range [45]. These results show that the sensitivity of transmission measurements is adequate for imaging burn injuries. With a reflection system THz radiation can be used to sense the "liquid" underneath skin samples.

3.3 Amino-acid Measurements

Fourier Transform Infrared (FTIR) spectroscopy is the most common used technique to observe the vibrational modes in biological structures. Compared to THz-TDS, FTIR spectroscopy has limitations about low frequency range that is generally between mid-infrared and far-infrared. Also, with the phase dependent results of THz-TDS measurements, refractive indices of biological samples could be investigated which is not possible with FTIR spectroscopy [51]].

Amino acids are the basis of the all metabolic processes and most of them are sensitive to THz waves in the low frequencies. Researches about different kind of amino acids in the THz range have been resulted in special absorption features that can be used as THz fingerprints to identify the type [52]].

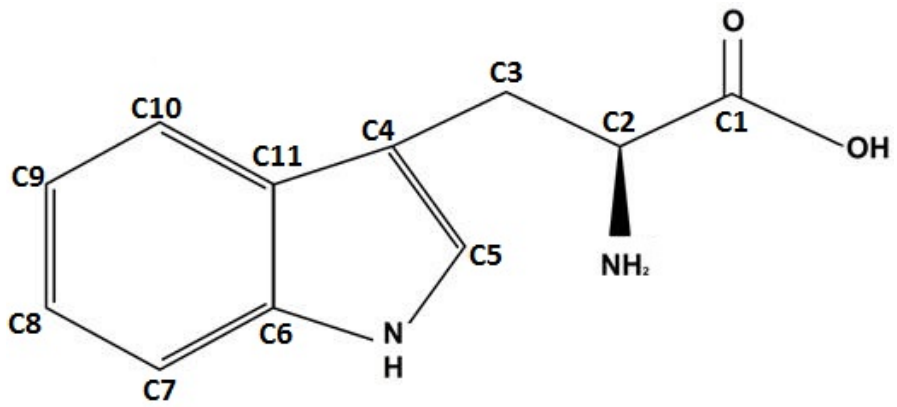

Figure 3.20: Skeletal formula of the L-Tryptophan

One of these amino acids is L- Tryptophan (L-Trp.) , Fig. 3.20 ,which is required to obtain from externally in case of lack of synthesizing. As the precursor of the serotonin L-Trp. is directly related with stress response, sleep, mood, and appetite regulation. Also, it has important roles in the protein biosynthesis and the chemical reactions in the cells. Variation of the L-Try concentrations during these processes could be a sign for some kind of diseases, for example, hematological neoplasias, adult T-cell leukemia, gastrointestinal cancer, and colorectal cancer are some of them that show an increase on tryptophan degradation. External sources for L-Trp. are a few vegetables, some commercial foods and,

some pharmaceuticals. To investigate the L-Trp. concentration various kind of techniques are used, such as; spectrophotometry, chemiluminescence, electro analytical methods, gas chromatography (GC), high-performance liquid chromatography (HPLC) [53].

3.3.1 THz-TDS Measurements

Polyethylene is a THz transparent material so, an ideal substrate to be used as host for L-Trp. measurements with THz-TDS. Spectrophotometric grade high density polyethylene and L-Trp. were supplied from Sigma-Aldrich (St. Louis, MO; No. 434272 and, MO; No. T-8659, respectively) by Department of Biology, METU. In an agate mortar L-Trp. and polyethylene were mixed until a homogenous mixture is obtained. Since the form of L-Trp. and polyethylene is more likely powder, samples are prepared as pellets by pressing with 1500 psi pressure for 10 minutes. Due to the aim of work, to observe the concentration change of L-Trp., different concentration rates were determined with respect to the weight. Thicknesses of the sample are the most critical point for THz-TDS because of the transmission geometry. Therefore10 and 25 % tryptophan containing polyethylene pellets with 0.42mm and 0.43mm thicknesses were prepared. In addition to concentration based sample, pure polyethylene and pure tryptophan references were used as negative and positive control samples with a 0.49mm and 0.71mm thicknesses respectively.

Time shift of increased ratio of tryptophan is observed in THz waveforms of the samples proportionally. In the time domain 10% of tryptophan is not adequate for the time shift from the pure polyethylene sample, but 25% of tryptophan is enough for a significant time delay with respect to the pure polyethylene sample. Also, absorption of the THz signal can be seen for both ratios.

The increase of the refractive index is proportional with the tryptophan concentration. Reference samples have the highest and lowest refractive indices; about 1.42 and 1.84 that belongs to in order of pure tryptophan and polyethylene. With the reference measurements the limits of the refractive indices are determined and afterwards refractive indices of samples with different concentrations

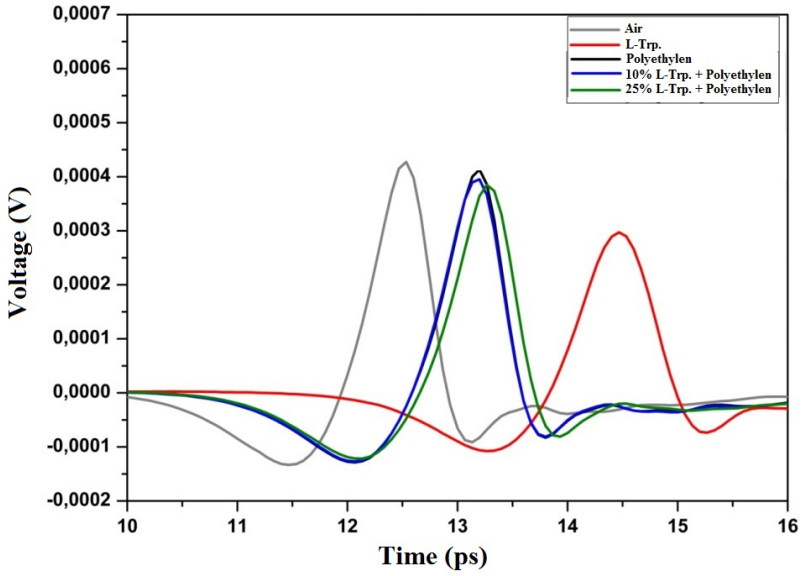

Figure 3.21: THz scans of concentration based and reference samples

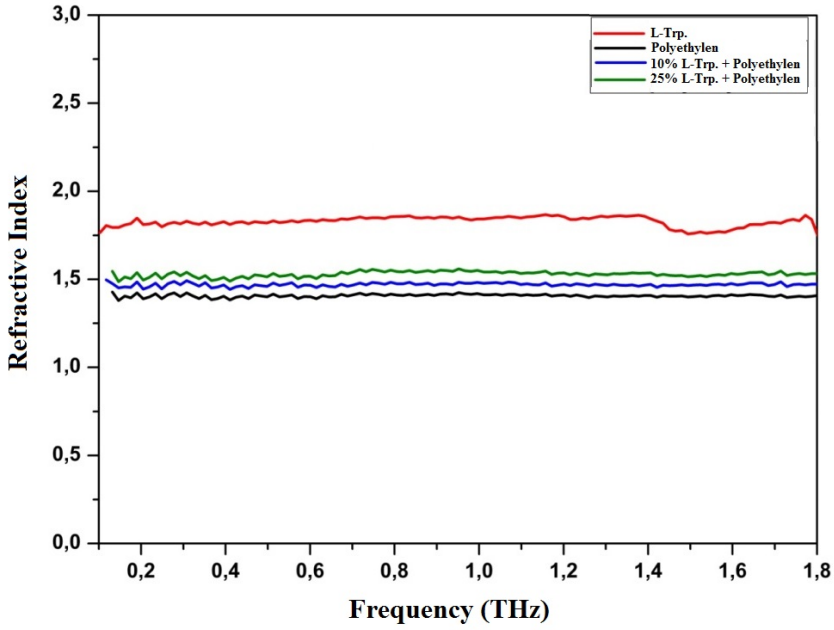

Figure 3.22: Refractive indices of concentration based and reference samples

are expected between 1.42 and 1.84 as 0% and 100% concentrations. The approximate refractive index values for 10% and 25% of tryptophan samples were measured as 1.48 and 1.54 at 1THz respectively.

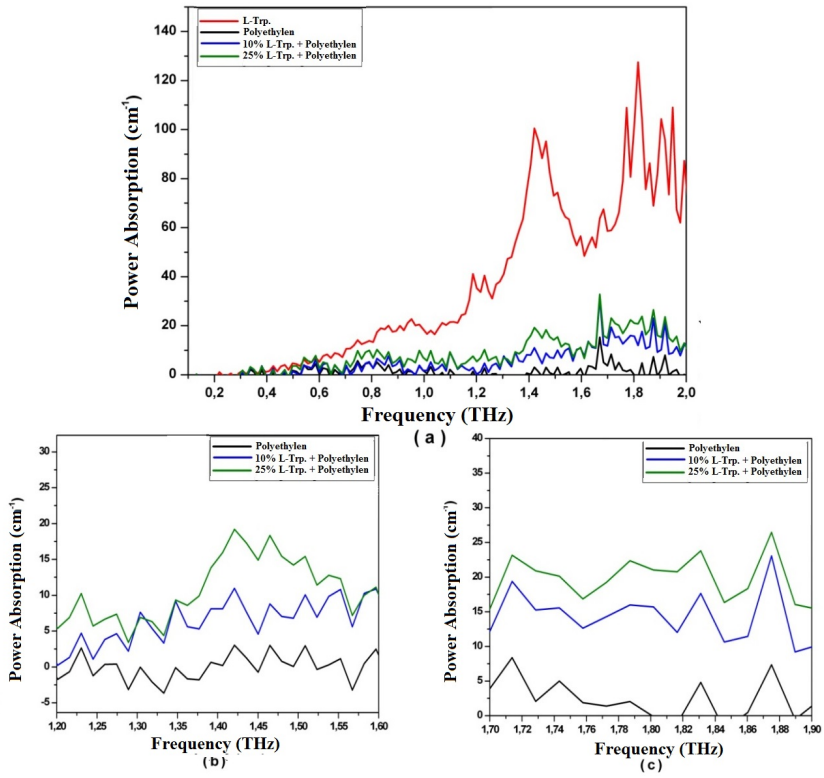

Figure 3.23: Absorption coefficient between (a) 0.1-2THz (b) 1.2-1.6THz and (c) 1.7-1.9THz

In Fig. 3.3.1.2 (a) special absorption features of pure tryptophan is observed at 1.42 THz and 1.82 THz between 0.1 THz and 2 THz. The reason of the first peak at 1.42 THz is based on the torsional motion of C11 and C12 in the tryptophan molecule. On the other hand, the second peak at the 1.82 THz is correlated to the ring torsions of C1 – C9. [54] Inferences of the measurement are consistent with the literature reviews of L-Trp. measurements which resulted with the observation of the peaks at 1.44THz and 1.84THz [55]. To investigate the proportional change at power absorptions of the concentration based samples, closer views of the peaks are evaluated in the ranges of 1.2-1.6THz and 1.7-1.9THz in Fig. 3.23 (b) and (c). Absorption coefficients of polyethylene, 10% tryptophan sample, 25% tryptophan sample and, pure tryptophan are 3.02, 10.97, 19.2 and, 100.5 at 1,42THz and 0.5, 11.9, 21.1 and, 127.5 at 1.82THz respectively. Hence

observation of the low percentage of tryptophan concentration is possible with the sensitivity of THz waves. Approximate values that are obtained from the concentration based measurements for refractive indices and power absorptions are given as a summary in Table 3.2 that shows the increase of the refractive index and power absorption values with respect to the percentage of the L-Trp in samples clearly.

Sample Definition	Thickness [mm]	Refractive Index	Power Absorption [cm^{-1}] at 1.42THz	Power Absorption [cm^{-1}] at 1.82THz
Polyethylen	0,49	1,42	3,02	0,5
Sample with 10% of L-Trp.	0,42	1,48	10,97	11,9
Sample with 25% of L-Trp.	0,43	1,54	19,2	21,1
Pure L-Trp.	0,71	1,84	100,5	127,5

Table3.2: Results of the reference and concentration dependent sample measurements

3.3.2 Results and Discussion

THz-TDS is used to identify the biological molecules with the reference of the intermolecular vibrations. L-Trp. is a known amino acid that has THz special fingerprints at 1.44THz and 1.84THz. Detection sensitivity of THz waves through the low concentration samples is investigated with the measurements of different percentage of L-Trp. content in a dry polyethylene host. The results of the measurements are consistent with respect to the concentration of L-Trp. for both refractive index and power absorption. Also, absorption features, which have been attributed to the torsional motion of C11 and C12 and the ring torsions of C1 – C9, are observed at in order of 1.42 THz and 1.82 THz [54].

The Complex Refractive Index Model (CRI) is used to understand the relation between the tryptophan concentrations of the samples and refractive and absorptive properties. The effect of the volumetric contents on refractive index is explained with CRI model for mixed samples [56].

$$\widetilde{n} \widetilde{=} f_x \widetilde{n_x} + (1 - f_x)\widetilde{n_h} \tag{3.1}$$

With reference to the CRI model the linear relation of the host medium's refractive index and the volumetric concentration of the add-on component is given in Eq. 3.1, where $\widetilde{n}$ is the complex refractive index of mixture, f_x is volumetric fraction of add-on component (x), $\widetilde{n}_x$ is the complex refractive index of add-on component (x) and $\widetilde{n}_h$ is the complex refractive index of host medium [53]. For this work, host medium is polyethylene and the add-on component is tryptophan. Calculations for concentration based samples were done to obtain the refractive index in the frequency domain.

Actual volumetric concentration and volumetric fractions were calculated with the help of the mass and density values of the polyethylene (0.95g/ml) and tryptophan (0.902g/ml) from the data sheets. The volumetric fractions (x) of tryptophan and polyethylene were calculated as 0.095 and 0.905 for 10% of tryptophan sample and 0.208 and 0.792 for 25% of tryptophan sample, respectively. Calculations with the CRI model and the measured refractive indices of the reference samples was resulted with refractive index values of 1.45 for the 10% and 1.50 for the 25% mixture. Also, with respect to the peak absorption coefficients at 1.42 THz volumetric indices of 10% and 25% tryptophan samples for tryptophan and polyethylene were calculated as 0.082 and 0.918, 0.166 and 0.834with CRI model. The CRI model enables an analysis without the knowledge of sample thickness by analyzing the gradient of peak amplitudes during the transmissions of the THz pulse through samples. The results of the calculations are summarized in Table 3.3.

Outcome of the measurements shows that THz-TDS is a precise technique to detect the low concentration of L-Trp. and the gradient of the L-Trp. content. These results could be used for screening and diagnosis of cancer and pathological diseases.

		Actual volumetric concentration %	Volumetric concentration from real refractive index ±3 %	Volumetric concentration from power absorption coefficient ±5 %	Volumetric concentration from change in time-domain pulse amplitude ± 1 %
10% Tryptophan by weight	Tryptophan	9,50	13,50	8,20	14,40
	Polyethylene	90,50	86,50	91,80	85,60
25% Tryptophan by weight	Tryptophan	20,80	29,70	16,60	25,80
	Polyethylene	79,20	70,30	83,40	74,20

Table3.3: Summary of the CRI model calculations

CHAPTER 4

CONCLUSION

In this study, measurement of the biological samples with a THz-TDS system was performed and the interactions between the THz waves and soft tissues, hard tissues and, amino acids were investigated. Teeth samples, skin sample and, concentration based L-Trp. samples were used as hard tissue, soft tissue and, amino acid.

The refractive index and power absorption of the tooth samples were observed in the range of 0.1-1THz for wet and dry states. Lower refractive index and higher power absorption were found for wet samples with respect to the dry samples. Another remarkable result was the differences between the healthy tooth and tooth with caries because of the scattering from the decayed part of the tooth. In a specific region, between 0.1 THz and 0.5 THz, healthy samples had higher refractive indices and lower power absorptions compared to ones with caries. As a result of these measurements and analysis this technique could be applied to image the irregularities with great contrast in THz range and this could be a new application area for in-vivo diagnostics as an alternative to X-ray imaging.

1,2mm burned skin layer and 0.5ml water content underneath the skin sample was investigated to understand the sensitivity of THz radiation to the water concentration of burned injuries. The absorption coefficients of burned skin and burned skin with water had clear difference between 0.6 THz and 1THz. The sensitivity of the THz-TDS system shows that THz waves could be used to identify the liquid content underneath the burned part of the skin with reflection geometry.

Different concentrations of L-Trp. samples with polyethylene as host were analyzed to understand the sensitivity of THz waves to amino acid molecules. Proportional increase of the refractive index and power absorption with the increasing L-Trp. content was found. Also, power absorption at 1.42THz and 1.82THz were observed as the torsional motion of C11 and C12 and the ring torsions of C1 – C9. with CRI model the linear relation of the refractive index of polyethylene and the volumetric concentration of tryptophan was analyzed. Results of the measurements show that THz-TDS is as sensitive as to identify the concentration of L-Trp. and to observe the change of the L-Trp. content. Therefore THz-TDS could be used for screening of biological molecules and diagnosis of some diseases that show variations on L-Trp. concentration.

REFERENCES

[1] K.-E. Peiponen, A. Zeitler, and M. Kuwata-Gonokami, *Terahertz spectroscopy and imaging*, vol. 171. Springer, 2012.

[2] Z. D. Taylor, R. S. Singh, D. B. Bennett, P. Tewari, C. P. Kealey, N. Bajwa, M. O. Culjat, A. Stojadinovic, H. Lee, J.-P. Hubschman, *et al.*, "Thz medical imaging: in vivo hydration sensing," *Terahertz Science and Technology, IEEE Transactions on*, vol. 1, no. 1, pp. 201–219, 2011.

[3] J. C. Wiltse, "History of millimeter and submillimeter waves," *Microwave Theory and Techniques, IEEE Transactions on*, vol. 32, no. 9, pp. 1118–1127, 1984.

[4] P. H. Siegel, "Terahertz pioneer: David h. auston," *IEEE Transactions on Terahertz Science and Technology*, vol. 1, no. 1, pp. 6–8, 2011.

[5] Y. Sun, M. Y. Sy, Y.-X. J. Wang, A. T. Ahuja, Y.-T. Zhang, and E. Pickwell-MacPherson, "A promising diagnostic method: Terahertz pulsed imaging and spectroscopy," *World journal of radiology*, vol. 3, no. 3, p. 55, 2011.

[6] D. Grischkowsky, S. Keiding, M. Van Exter, and C. Fattinger, "Far-infrared time-domain spectroscopy with terahertz beams of dielectrics and semiconductors," *JOSA B*, vol. 7, no. 10, pp. 2006–2015, 1990.

[7] H. C. B. Skjeie, "Terahertz time-domain spectroscopy," 2012.

[8] B. Jin, C. Zhang, P. Wu, and S. Liu, "Recent progress of terahertz spectroscopy on medicine and biology in china," *Terahertz Sci. Technol*, vol. 3, no. 4, pp. 192–200, 2010.

[9] G. J. Wilmink and J. E. Grundt, "Invited review article: current state of research on biological effects of terahertz radiation," *Journal of Infrared, Millimeter, and Terahertz Waves*, vol. 32, no. 10, pp. 1074–1122, 2011.

[10] A. Fitzgerald, E. Berry, N. Zinov'ev, S. Homer-Vanniasinkam, R. Miles, J. Chamberlain, and M. Smith, "Catalogue of human tissue optical properties at terahertz frequencies," *Journal of Biological Physics*, vol. 29, no. 2-3, pp. 123–128, 2003.

[11] R. Miles, X.-C. Zhang, H. Eisele, and A. Krotkus, *Terahertz frequency detection and identification of materials and objects*. Springer Science & Business Media, 2007.

[12] J.-B. Masson, M.-P. Sauviat, J.-L. Martin, and G. Gallot, "Ionic contrast terahertz near-field imaging of axonal water fluxes," *Proceedings of the National Academy of Sciences of the United States of America*, vol. 103, no. 13, pp. 4808–4812, 2006.

[13] X. Yin, B. W.-H. Ng, and D. Abbott, *Terahertz imaging for biomedical applications: pattern recognition and tomographic reconstruction.* Springer Science & Business Media, 2012.

[14] E. R. Mueller, "Terahertz radiation sources for imaging and sensing applications-new techniques are being used to generate emissions at terahertz frequencies.," *Photonics Spectra*, vol. 40, no. 11, pp. 60–69, 2006.

[15] I. Wilke and S. Sengupta, "Nonlinear optical techniques for terahertz pulse generation and detection—optical rectification and electrooptic sampling," *Terahertz Spectroscopy: Principles and Applications, Optical Science and Engineering*, vol. 131, p. 41, 2008.

[16] A. Rice, Y. Jin, X. Ma, X.-C. Zhang, D. Bliss, J. Larkin, and M. Alexander, "Terahertz optical rectification from$<$ 110$>$ zinc-blende crystals," *Applied physics letters*, vol. 64, no. 11, pp. 1324–1326, 1994.

[17] K. Yeh, M. Hoffmann, J. Hebling, and K. A. Nelson, "Generation of 10 j ultrashort terahertz pulses by optical rectification," *Appl. Phys. Lett*, vol. 90, no. 171121, pp. 1–3, 2007.

[18] J. Rowley, J. Wahlstrand, K. Zawilski, P. Schunemann, N. Giles, and A. Bristow, "Terahertz generation by optical rectification in uniaxial birefringent crystals," *Optics Express*, vol. 20, no. 15, pp. 16968–16973, 2012.

[19] V. Apostolopoulos and M. Barnes, "Thz emitters based on the photodember effect," *Journal of Physics D: Applied Physics*, vol. 47, no. 37, p. 374002, 2014.

[20] X.-C. Zhang and J. Xu, *Introduction to THz wave photonics.* Springer, 2010.

[21] S. Kono, P. Gu, M. Tani, and K. Sakai, "Temperature dependence of terahertz radiation from n-type insb and n-type inas surfaces," *Applied Physics B*, vol. 71, no. 6, pp. 901–904, 2000.

[22] M. Herrmann, R. Fukasawa, and O. Morikawa, "Terahertz imaging," in *Terahertz Optoelectronics*, pp. 331–382, Springer, 2005.

[23] A. Rogalski and M. Razeghi, "Semiconductor ultraviolet photodetectors," *OPTOELECTRONICS REVIEW*, pp. 13–30, 1996.

[24] M. Tani, M. Herrmann, and K. Sakai, "Generation and detection of terahertz pulsed radiation with photoconductive antennas and its application to imaging," *Measurement science and technology*, vol. 13, no. 11, p. 1739, 2002.

[25] R. Paschotta, *Encyclopedia of laser physics and technology*, vol. 1. Wiley-vch Berlin, 2008.

[26] M. C. Beard, G. M. Turner, and C. A. Schmuttenmaer, "Terahertz spectroscopy," *The Journal of Physical Chemistry B*, vol. 106, no. 29, pp. 7146–7159, 2002.

[27] L. Duvillaret, F. Garet, and J.-L. Coutaz, "Highly precise determination of optical constants and sample thickness in terahertz time-domain spectroscopy," *Applied optics*, vol. 38, no. 2, pp. 409–415, 1999.

[28] Q. Zhou and X. Zhang, "Applications of time-resolved terahertz spectroscopy in ultrafast carrier dynamics," *Chinese Optics Letters*, vol. 9, no. 11, p. 110006, 2011.

[29] M. C. Beard, G. M. Turner, and C. A. Schmuttenmaer, "Transient photoconductivity in gaas as measured by time-resolved terahertz spectroscopy," *Physical Review B*, vol. 62, no. 23, p. 15764, 2000.

[30] R. A. Lewis and R. A. Lewis, *Terahertz physics*. Cambridge University Press, 2013.

[31] Batop, "Pca - photoconductive antenna for thz waves, 800 nm." `http://www.batop.de/products/terahertz/photoconductive-antenna/photoconductive-antenna-800nm.html`. Accessed December 20, 2015.

[32] N. Khiabani, *Modelling, design and characterisation of terahertz photoconductive antennas*. PhD thesis, University of Liverpool, 2013.

[33] A. Nahata, A. S. Weling, and T. F. Heinz, "A wideband coherent terahertz spectroscopy system using optical rectification and electro-optic sampling," *Applied Physics Letters*, vol. 69, no. 16, pp. 2321–2323, 1996.

[34] H. Bakker, G. Cho, H. Kurz, Q. Wu, and X.-C. Zhang, "Distortion of terahertz pulses in electro-optic sampling," *JOSA B*, vol. 15, no. 6, pp. 1795–1801, 1998.

[35] A. Nahata, D. H. Auston, T. F. Heinz, and C. Wu, "Coherent detection of freely propagating terahertz radiation by electro-optic sampling," *Applied physics letters*, vol. 68, no. 2, pp. 150–152, 1996.

[36] H.-B. Liu, H. Zhong, N. Karpowicz, Y. Chen, and X.-C. Zhang, "Terahertz spectroscopy and imaging for defense and security applications," *Proceedings of the IEEE*, vol. 95, no. 8, pp. 1514–1527, 2007.

[37] K. Imai, K. Kawase, H. Minamide, and H. Ito, "Achromatically injection-seeded terahertz-wave parametric generator," in *Terahertz Electronics Proceedings, 2002. IEEE Tenth International Conference on*, pp. 56–59, IEEE, 2002.

[38] M. Kelley, *Terahertz time domain spectroscopy of amino acids and sugars*. PhD thesis, Citeseer, 2013.

[39] P. U. Jepsen and B. M. Fischer, "Dynamic range in terahertz time-domain transmission and reflection spectroscopy," *Optics letters*, vol. 30, no. 1, pp. 29–31, 2005.

[40] Y. C. Sim, I. Maeng, and J.-H. Son, "Frequency-dependent characteristics of terahertz radiation on the enamel and dentin of human tooth," *Current Applied Physics*, vol. 9, no. 5, pp. 946–949, 2009.

[41] A. Lussi, N. Kohler, D. Zero, M. Schaffner, and B. Megert, "A comparison of the erosive potential of different beverages in primary and permanent teeth using an in vitro model," *European Journal of Oral Sciences*, vol. 108, no. 2, pp. 110–114, 2000.

[42] P. Bartold, "Dentinal hypersensitivity: a review," *Australian dental journal*, vol. 51, no. 3, pp. 212–218, 2006.

[43] P. Han, G. Cho, and X.-C. Zhang, "Time-domain transillumination of biological tissues with terahertz pulses," *Optics Letters*, vol. 25, no. 4, pp. 242–244, 2000.

[44] M. D. Peck, "Epidemiology of burns throughout the world. part i: Distribution and risk factors," *Burns*, vol. 37, no. 7, pp. 1087–1100, 2011.

[45] M. H. Arbab, T. C. Dickey, D. P. Winebrenner, A. Chen, M. B. Klein, and P. D. Mourad, "Terahertz reflectometry of burn wounds in a rat model," *Biomedical optics express*, vol. 2, no. 8, pp. 2339–2347, 2011.

[46] B. S. Atiyeh, S. W. Gunn, and S. N. Hayek, "State of the art in burn treatment," *World journal of surgery*, vol. 29, no. 2, pp. 131–148, 2005.

[47] J. Still, E. Law, K. Klavuhn, T. Island, and J. Holtz, "Diagnosis of burn depth using laser-induced indocyanine green fluorescence: a preliminary clinical trial," *Burns*, vol. 27, no. 4, pp. 364–371, 2001.

[48] M. H. Arbab, D. P. Winebrenner, T. C. Dickey, A. Chen, M. B. Klein, and P. D. Mourad, "Terahertz spectroscopy for the assessment of burn injuries in vivo," *Journal of biomedical optics*, vol. 18, no. 7, pp. 077004–077004, 2013.

[49] P. Tewari, C. P. Kealey, D. B. Bennett, N. Bajwa, K. S. Barnett, R. S. Singh, M. O. Culjat, A. Stojadinovic, W. S. Grundfest, and Z. D. Taylor, "In vivo terahertz imaging of rat skin burns," *Journal of biomedical optics*, vol. 17, no. 4, pp. 0405031–0405033, 2012.

[50] Z. Taylor, R. Singh, M. Culjat, J. Suen, W. Grundfest, H. Lee, and E. Brown, "Reflective terahertz imaging of porcine skin burns," *Optics letters*, vol. 33, no. 11, pp. 1258–1260, 2008.

[51] M. Van Exter and D. R. Grischkowsky, "Characterization of an optoelectronic terahertz beam system," *Microwave Theory and Techniques, IEEE Transactions on*, vol. 38, no. 11, pp. 1684–1691, 1990.

[52] B. Jin, C. Zhang, P. Wu, and S. Liu, "Recent progress of terahertz spectroscopy on medicine and biology in china," *Terahertz Sci. Technol*, vol. 3, no. 4, pp. 192–200, 2010.

[53] Z. Özer, S. Gök, H. Altan, and F. Severcan, "Concentration-based measurement studies of l-tryptophan using terahertz time-domain spectroscopy (thz-tds)," *Applied spectroscopy*, vol. 68, no. 1, pp. 95–100, 2014.

[54] B. Yu, F. Zeng, Y. Yang, Q. Xing, A. Chechin, X. Xin, I. Zeylikovich, and R. Alfano, "Torsional vibrational modes of tryptophan studied by terahertz time-domain spectroscopy," *Biophysical Journal*, vol. 86, no. 3, pp. 1649–1654, 2004.

[55] A. Fitzgerald, E. Berry, N. Zinovev, G. Walker, M. Smith, and J. Chamberlain, "An introduction to medical imaging with coherent terahertz frequency radiation," *Physics in Medicine and biology*, vol. 47, no. 7, p. R67, 2002.

[56] M. Scheller, C. Jansen, M. Koch, *et al.*, *Applications of effective medium theories in the terahertz regime*. INTECH Open Access Publisher London, 2010.